183

Abstract

Current operational assimilation methods have revealed deficiencies in cases of strong baroclinic development. Baroclinic conditions are therefore appropriate for evaluating the potential of improvement which could be achieved through the implementation of a fully four-dimensional data assimilation. In this paper, the behaviour of a variational scheme is investigated for a typical baroclinic instability problem, where a wave develops and retroacts onto the basic zonal flow. The tangent linear model is shown to lead to a good approximation of the time evolution of the wave over a range of 48 hours, even at the most intense cyclogenesis period. For the assimilation experiments, the twin experiment approach is applied. Only part of the flow evolution is observed, either the zonal component or the eddy component. In either case, the method proves successful in reconstructing the unobserved part of the flow, taking advantage of the nonlinear coupling that exists between those components. However, nonlinearities can lead to difficulties when the range of validity of the tangent linear model is exceeded or when the cost function exhibits multiple minima.

1 Introduction.

On Thursday and Friday 15-16 October 1987, a severe storm devastated Brittany, Normandy and the south of England. An interesting behaviour of the ECMWF operational system at that time is that the medium range forecasts of the intensity of the storm were significantly better than that of the 36 hour forecast. The low was forecast at 955 hPa, 958 hPa and 954 hPa in the 108 h, 84 h and 60 h forecasts respectively, whereas at the 36 h range, it was 985 hPa (Jarraud et al. (1989)). The best manual analysis gives a low around 950 hPa. On the other hand, the trajectory of the storm was better predicted at the short range than at the medium range.

As the storm was present in the medium range forecasts, the models were able to represent the phenomenon, it is then likely that weaknesses of the data assimilation schemes are responsible for the poor 36 h forecasts. Lorenc et al. (1988) investigated the behaviour of the United-Kingdom Meteorological Office data assimilation schemes. They found a significant impact of late AIREP reports but also a "very large sensitivity to the details of the three-dimensional atmospheric structure which were not resolved by the available observations". This is typically a situation where the scheme used for blending the first-guess and the new data is of utmost importance and also where the weaknesses are revealed. Indeed, if there are a lot of observations, the analysis will fit the observations, but on the other hand if there are no data, it will stick to the first-guess. In addition Jarraud et al. (1989) pointed out that the large inconsistencies, at short range, between ECMWF and Météo-France operational models is another strong indication of data assimilation problems.

One immediately thinks of two strong simplifications made in the statistical model used in operational implementations of Optimal Interpolation : i) the separability between the horizontal and the vertical and ii) the spatial stationarity of the horizontal structure functions. In baroclinic conditions those hypotheses are certainly not valid. Meteorological situations with intense baroclinicity are then appropriate conditions in which to evaluate the potential for improvement which could be achieved through the implementation of a fully four-dimensional data assimilation (either four-dimensional variational scheme or Kalman filter).

Thépaut and Courtier (1991) (herein referred to as TC91) have demonstrated the numerical feasibility of four-dimensional variational data assimilation (4D-VAR) using a multilevel primitive-equation model, these results being confirmed by Navon et al. (1991). In addition, the former have presented some encouraging results on the synergistic behaviour of the consistent use of the dynamical information and of the observational information. The purpose of this paper is to investigate the behaviour of 4D-VAR in conditions in which the dynamics of the flow evolution are well understood and documented. It has to be considered as a preliminary study before using real observations in order to understand how the behaviour of 4D-VAR may depend on the dynamics.

We have chosen the typical baroclinic instability problem studied by Simmons and Hoskins (1978) (hereafter referred to as SH78). Section 2 presents the "meteorological situation", and in section 3 the linearity of the flow is studied. The results of the assimilation experiments are presented in section 4, and a discussion concludes the paper in section 5. The notations used here are the same as in TC91, in particular we refer to

that paper and references therein for a theoretical introduction to the data assimilation problem.

2 The baroclinic instability case.

2.a The meteorological situation.

The life cycle of a baroclinic wave on the sphere (SH78) is chosen as it represents one of the main features of mid-latitudes atmospheric dynamics. The basic zonal flow, chosen to be symmetric about the equator, is presented in Fig. 1. A baroclinic zone centered at 45° latitude is characterized by a horizontal temperature gradient with a ground-level temperature variation of $20K$ from 30° to 60°, in geostrophic balance with a tropospheric jet whose maximum reaches $36ms^{-1}$ at $150hPa$. This jet is baroclinically unstable and, for each zonal wavenumber the linearly most unstable mode can be determined as the mode emerging after a long-range integration of a numerical model maintained in the linear regime. As in SH78 or in Thorncroft and Hoskins (1990), zonal wavenumber six was chosen because, firstly, it is among the fastest growing modes and, secondly, because its wavelength (4700 km at mid-latitudes) is close to the observed horizontal size of large-scale cyclones.

As in TC91, the primitive equation model used in this study is the ARPEGE/IFS code developed through a cooperation between Météo-France and ECMWF (see TC91 for a brief description and Courtier et al.,1991 for a comprehensive one). The vertical discretization consists of the 19 levels of the hybrid pressure / σ vertical coordinate (Simmons and Burridge, 1981) of the 1990 operational ECMWF model , and in most experiments a T21 triangular truncation of the spherical harmonics representation of the fields is used, which represents 28072 degrees of freedom. The nonlinear evolution of the baroclinic wave is simulated by integrating the model for fifteen days from initial conditions consisting of the zonal flow perturbed by the most unstable mode at zonal wavenumber six. This mode is scaled so as to give $1hPa$ maximum amplitude for the surface pressure perturbation at the beginning of the integration.

The results are consistent with SH78: after nine days of growth during which the minimum value of the surface pressure drops from $1008hPa$ to $972hPa$, the reduction in baroclinicity of the flow and barotropic effects induce a decay of the wave and a corresponding increase of the maximum value of the zonal wind. As can be seen from Fig. 2 (compare with figure 13.12, panel b in Gill,1982 p579), the jet reaches $38ms^{-1}$ at the end of the period at truncation T21 ($41ms^{-1}$ at truncation T42, not shown). In the lower troposphere, the zonal part of the flow is also considerably altered by the wave : the temperature gradient is weakened and, as predicted by quasi-geostrophic theory (Gill,1982 chapter 13), westerly winds created below the jet are surrounded by easterlies. The most intense cyclogenesis occurs between days 6 and 8 with a maximum drop in surface pressure of 8 hPa per day. On the seventh day of the life cycle, the wave exhibits a structure characteristic of occluding systems at midlatitudes (Fig. 3 to be compared with Fig. 1 of SH78 or Fig. 13.12,panel c in Gill,1982 p579). In the following, we shall concentrate on the 24 h period starting at day 6.

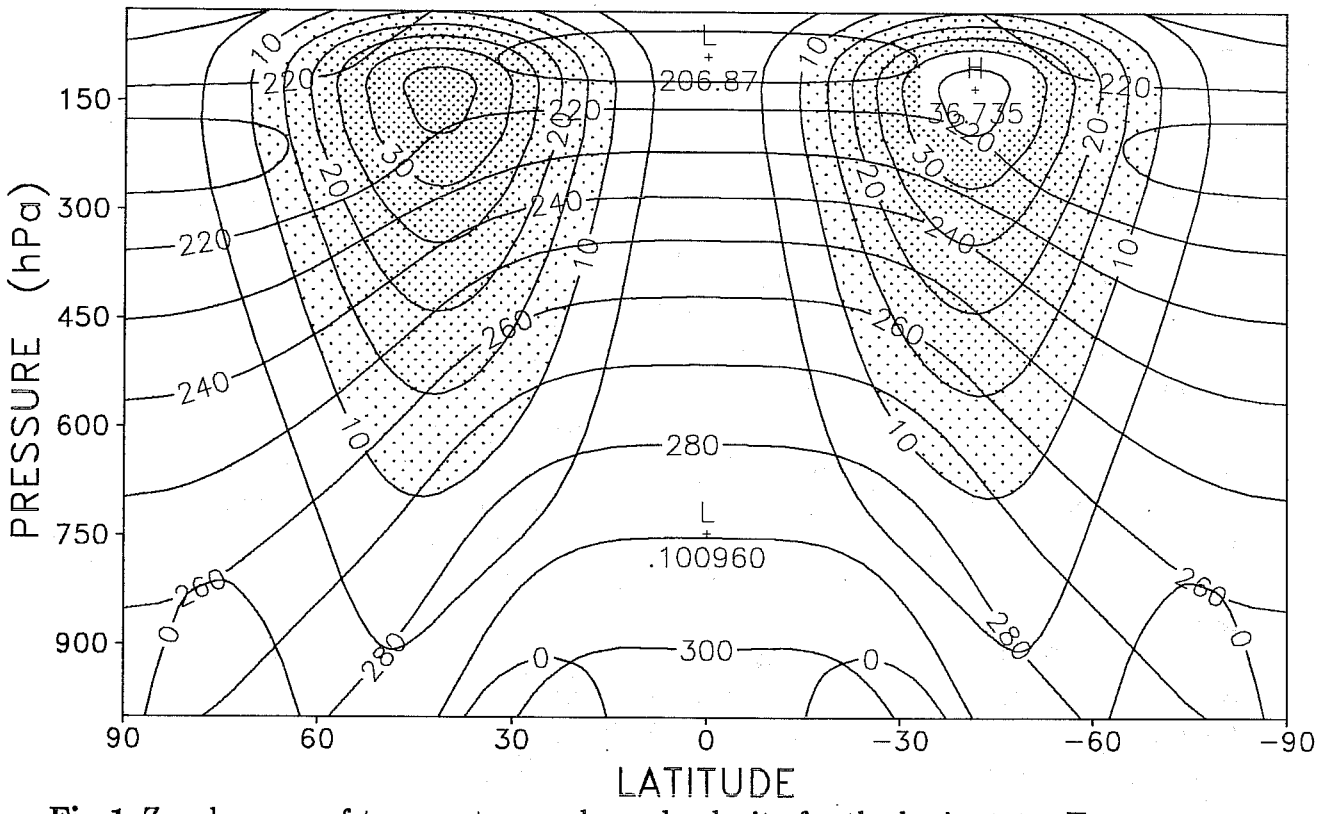

Fig.1 Zonal means of temperature and zonal velocity for the basic state. Temperature contours are drawn every $10K$ and zonal velocity contours are drawn every $5ms^{-1}$. Areas where winds exceed $10ms^{-1}$ are shaded.

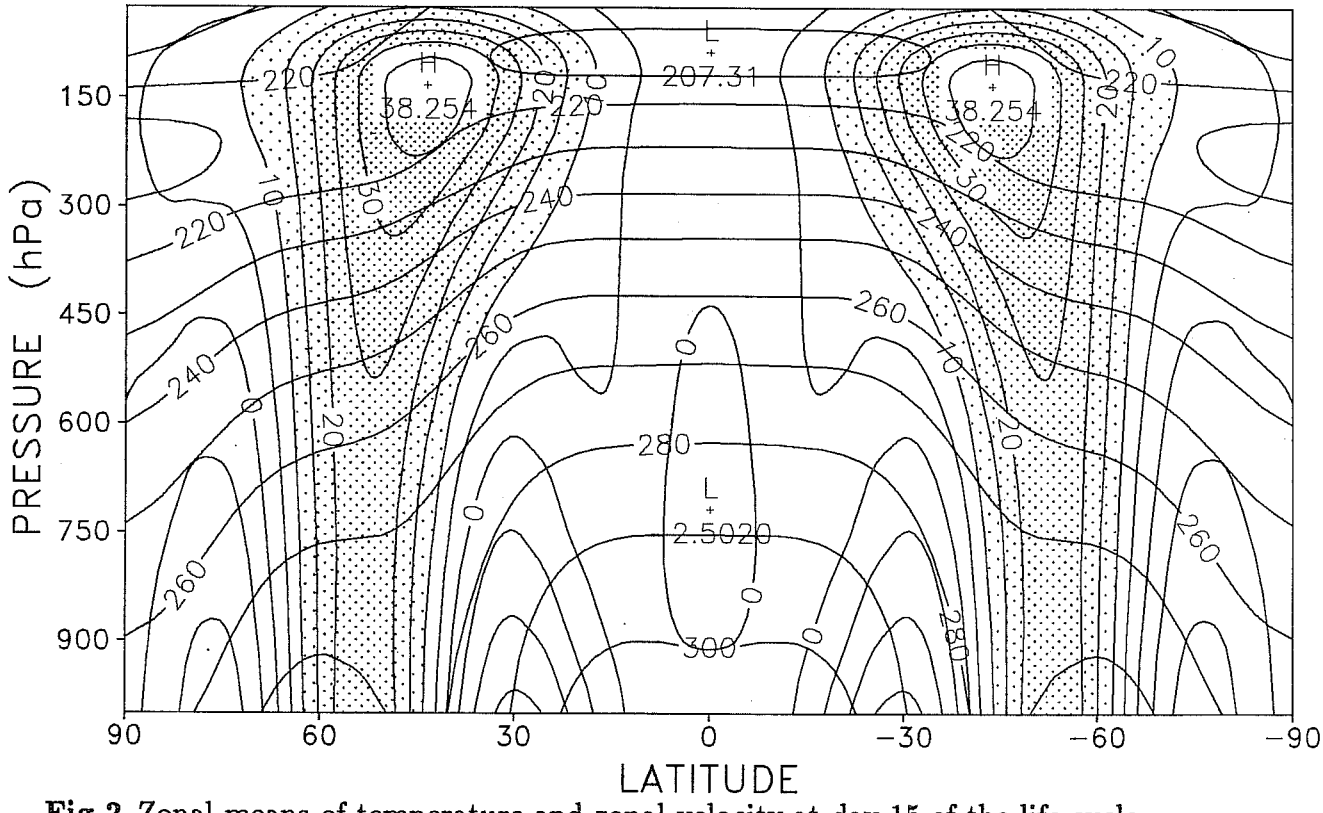

Fig.2 Zonal means of temperature and zonal velocity at day 15 of the life cycle.

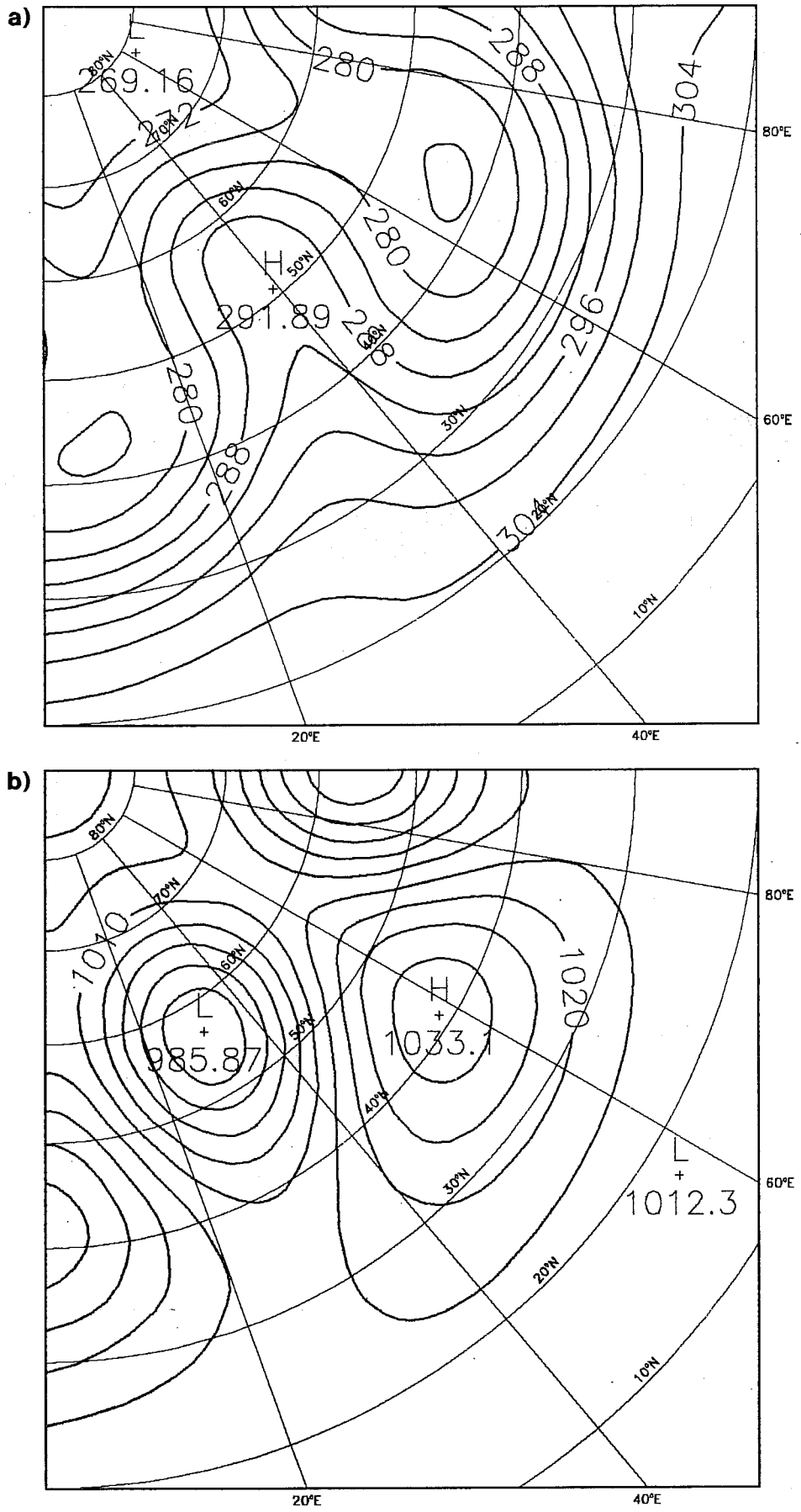

Fig.3 Temperature at the lowest level (panel(a)) and surface pressure (panel(b)), at day 7. Contour intervals are $4K$ for the temperature and $5hPa$ for the surface pressure.

2.b Some theoretical results.

Let us consider the tangent-linear model obtained by linearization in the vicinity of a trajectory $x(t)$ of the full nonlinear model. Assuming that the initial conditions $x(t_0)$ of this trajectory consist of zonal fields and that the model is invariant under rotation, it is shown in appendix 1 that the resolvent $\mathcal{R}(t_n, t_0)$ keeps invariant any Fourier subspace E_m consisting of model state perturbations of zonal wave number m. In other words, the dynamics of the tangent linear equation obtained by linearization in the vicinity of a zonal trajectory is independent from one m to another, the matrix of the resolvent is block diagonal. This result is an immediate consequence of the fact that the resolvent $\mathcal{R}(t_n, t_0)$ commutes with any zonal rotation R_z^θ through angle θ.

Similarly, if the initial conditions $x(t_0)$ are chosen symmetric about the equator as in the present paper, the evolutions given by the resolvent of the symmetric and antisymmetric part of the flow are independent.

If the initial conditions $x(t_0)$ of the trajectory $x(t)$ are no longer zonal but only limited to zonal wave numbers (0, 6, 12, 18...), the trajectory is invariant by the rotation $R_z^{\frac{2\pi}{6}}$. The resolvent commutes with this rotation and using the same proof as in appendix 1, the six subspaces $E_{m+6k}, (k = 0, 1, 2, ...)$ for m varying between 0 and 5, are kept invariant by the resolvent. A given zonal wave number m interacts only with its harmonics $m + 6k$.

3 Linearity of the flow.

In this section, we address the question of how important the influence of nonlinear terms is, on the evolution of the flow. This preliminary study of the relative linearity of the dynamics will help in understanding and tackling the assimilation problem. As already studied by Lacarra and Talagrand (1988), this question is of primary importance for data assimilation since, from a theoretical point of view if the dynamics are linear, 4D-VAR is equivalent to the Kalman filter, and the result of the assimilation is the Best Linear Unbiased Estimator (BLUE). In addition, from a practical point of view, linearity ensures quadraticity of the cost function to be minimized, which generally improves the behaviour of descent algorithms. This is no longer true for strongly nonlinear situations as Gauthier (1991) has shown in chaotic situations using the Lorenz model.

Starting from day 6 of the life cycle, the nonlinear evolution of the perturbation is compared to its linear evolution as given by the tangent linear model. At time t_0, let us write the atmospheric state vector as

$$x(t_0) = x_0(t_0) + \delta x(t_0) \tag{1}$$

where $x_0(t_0)$ stands for the basic state and $\delta x(t_0)$ for the perturbation. The basic state is chosen as the zonal part of the flow described in the previous section taken at day 6 and the perturbation as its eddy part. The amplitude of the initial perturbation $\delta x(t_0)$ is then far from being negligible: at 55° latitude, the surface pressure amplitude is $20hPa$, and that of the temperature at the lowest level is $10K$. The evolution of x is given by the integration of the model $\mathcal{M}$ between times t_0 and t_n

$$x(t_n) = \mathcal{M}(t_n, t_0)(x(t_0)) = \mathcal{M}(t_n, t_0)(x_0(t_0) + \delta x(t_0)) \tag{2}$$

whereas the first order evolution of the perturbation $\delta x(t_0)$ is the result of the integration of the tangent linear model $\mathcal{R}$ obtained by linearisation of the nonlinear model $\mathcal{M}$ in the vicinity of the trajectory whose initial condition is the basic state $x_0(t_0)$

$$\delta x(t_n) = \mathcal{R}(t_n, t_0)\delta x(t_0). \tag{3}$$

As a remark, it should be noted that the basic state $x_0(t_0)$ is almost stationary. Its own evolution, as measured by the energy of the difference $x_0(t_0 + 24h) - x_0(t_0)$, is 6 orders of magnitude smaller than the evolution of the zonal part of the flow when the perturbation is included. Thus, the coefficients of the tangent linear model are almost constant. However, all the computations were carried out with the exact definition of the tangent linear model linearised in the vicinity of the genuine trajectory.
The Taylor formula leads to

$$\left.\begin{aligned} \mathcal{M}(t_n, t_0)(x_0(t_0) + \delta x(t_0)) &= \mathcal{M}(t_n, t_0)(x_0(t_0)) + \mathcal{R}(t_n, t_0)\delta x(t_0) \\ &+ \tfrac{1}{2!}\mathcal{H}\delta x(t_0)^2 + \tfrac{1}{3!}\mathcal{P}_3\delta x(t_0)^3 \\ &+ \tfrac{1}{4!}\mathcal{P}_4\delta x(t_0)^4 + \tfrac{1}{5!}\mathcal{P}_5\delta x(t_0)^5 + ... \end{aligned}\right\} \tag{4}$$

where $\mathcal{H}$ denotes the second derivatives of $\mathcal{M}$ and $\mathcal{P}_3$, $\mathcal{P}_4$, $\mathcal{P}_5$ ... denote the derivatives of $\mathcal{M}$ of respective order 3, 4, 5 ... We compare the total perturbation

$$\left.\begin{aligned}\mathcal{N}(\delta x(t_0)) &= \mathcal{M}(t_n,t_0)(x_0(t_0)+\delta x(t_0)) - \mathcal{M}(t_n,t_0)(x_0(t_0)) \\ &= \mathcal{R}(t_n,t_0)\delta x(t_0) + \tfrac{1}{2!}\mathcal{H}\delta x(t_0)^2 + ...\end{aligned}\right\} \tag{5}$$

to its linear component

$$\mathcal{L}(\delta x(t_0)) = \mathcal{R}(t_n,t_0)\delta x(t_0). \tag{6}$$

The difference between the two

$$\mathcal{D}(\delta x(t_0)) = \mathcal{N}(\delta x(t_0)) - \mathcal{L}(\delta x(t_0)) = \frac{1}{2!}\mathcal{H}\delta x(t_0)^2 + \frac{1}{3!}\mathcal{P}_3\delta x(t_0)^3 + ... \tag{7}$$

is split into its odd and even components

$$\mathcal{O}(\delta x(t_0)) = \frac{1}{2}(\mathcal{D}(\delta x(t_0)) - \mathcal{D}(-\delta x(t_0)) = \frac{1}{3!}\mathcal{P}_3\delta x(t_0)^3 + \frac{1}{5!}\mathcal{P}_5\delta x(t_0)^5 + ... \tag{8}$$

$$\mathcal{E}(\delta x(t_0)) = \frac{1}{2}(\mathcal{D}(\delta x(t_0)) + \mathcal{D}(-\delta x(t_0)) = \frac{1}{2!}\mathcal{H}\delta x(t_0)^2 + \frac{1}{4!}\mathcal{P}_4\delta x(t_0)^4 + ... \tag{9}$$

In order to quantify the relative importance of $\mathcal{L}$, $\mathcal{D}$, $\mathcal{O}$ and $\mathcal{E}$, it is necessary to introduce a notion of norm in phase space. As in TC91, we have chosen the quadratic invariant energy of the primitive equations linearised in the vicinity of a state of rest. The square of the norm $\| x \|^2$ of a field x is given by

$$\left.\begin{aligned}\| x \|^2 = \frac{1}{2}\int_0^1\iint_\Sigma (&\nabla\Delta^{-1}\zeta\cdot\nabla\Delta^{-1}\zeta + \nabla\Delta^{-1}D\cdot\nabla\Delta^{-1}D \\ &+R_aT_r(ln\pi)^2 + \frac{C_p}{T_r}T^2)d\Sigma(\frac{\partial p}{\partial\eta})d\eta\end{aligned}\right\} \tag{10}$$

where ζ, D, T and π stand for vorticity, divergence, temperature and surface pressure fields, T_r for the reference temperature, η for the vertical coordinate and R_a and C_p for the thermodynamical constants.

One sees from Eq. 10 that the zonal and eddy parts of a given state are orthogonal. The total squared norm can then be split into its zonal and eddy contributions. As a matter of fact, the perturbation is chosen as a pure eddy at time t_0 but its temporal evolution is twofold: the evolution of the eddy part itself and a retroaction onto the zonal part of the flow. Fig. 4 shows the ratios of all the following quantities: $\frac{\|\mathcal{D}\|}{\|\mathcal{L}\|}$, $\frac{\|\mathcal{O}\|}{\|\mathcal{L}\|}$ and $\frac{\|\mathcal{E}\|}{\|\mathcal{L}\|}$. Panel (a) is relative to the evolution of the eddy contribution of the norms and panel (b) to the total norms.

The ratio of the nonlinear term ($\mathcal{D}$) to the linear term ($\mathcal{L}$) (full curve of panel (a)) reaches 7.3 %, 24.1 % and 48.8 % at the respective ranges of 24 h, 48 h and 72 h for the eddy part of the flow. This shows that the tangent linear model describes to a good

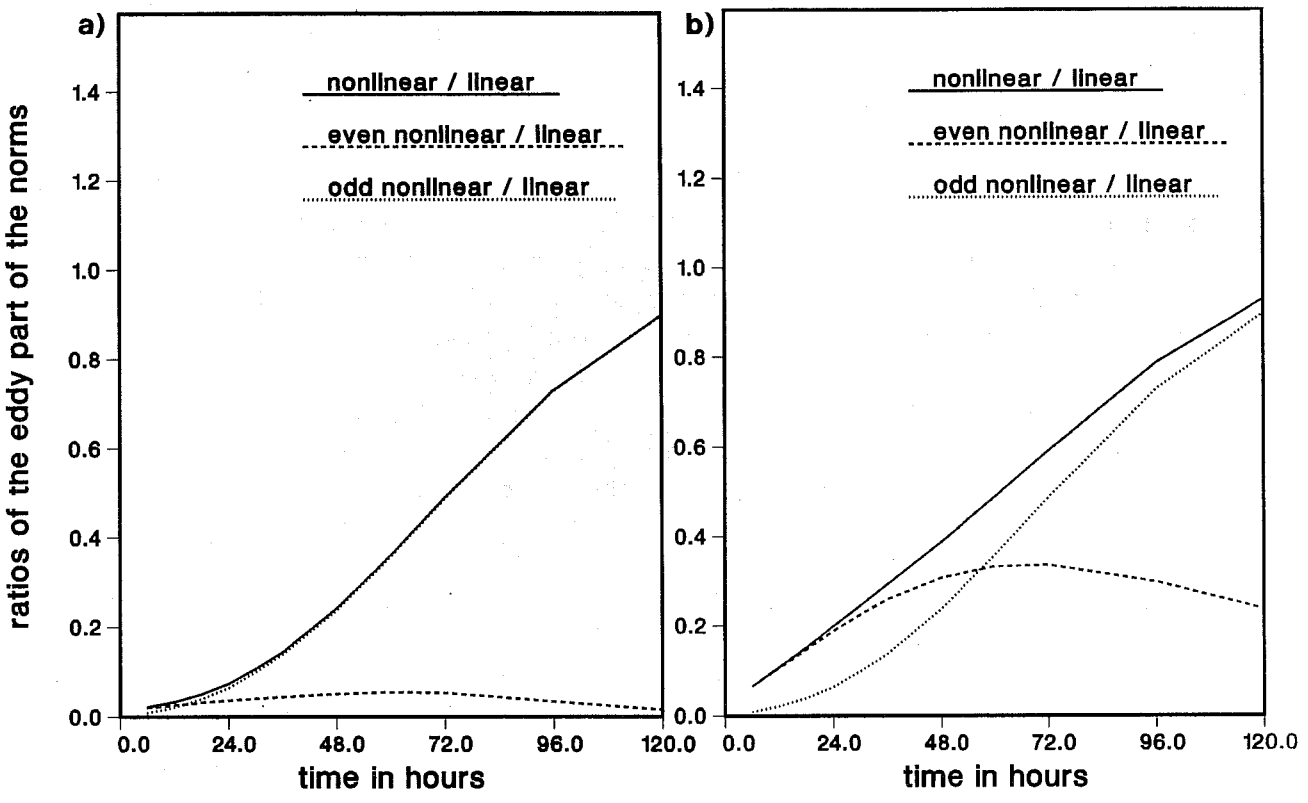

Fig.4 Ratios quantifying the degree of nonlinearity of the evolution of the perturbation ($\delta x(t_0)$) according to time, starting at day 6.

Full curve is the ratio of the nonlinear component of the perturbation to its linear component: $\frac{\|\frac{1}{2!}\mathcal{Q}\delta x(t_0)^2+\frac{1}{3!}\mathcal{P}_3\delta x(t_0)^3+....\|}{\|\mathcal{R}(t_1,t_0)\delta x(t_0)\|}$

Dotted curve is the ratio of the odd nonlinear component of the perturbation to its linear component: $\frac{\|\frac{1}{3!}\mathcal{P}_3\delta x(t_0)^3+\frac{1}{5!}\mathcal{P}_5\delta x(t_0)^5+....\|}{\|\mathcal{R}(t_1,t_0)\delta x(t_0)\|}$

Dashed curve is the ratio of the even nonlinear component of the perturbation to its linear component: $\frac{\|\frac{1}{2!}\mathcal{Q}\delta x(t_0)^2+\frac{1}{4!}\mathcal{P}_4\delta x(t_0)^4+....\|}{\|\mathcal{R}(t_1,t_0)\delta x(t_0)\|}$

Panel (a) presents the ratios of the eddy parts of the norm (all zonal wavenumbers except $m = 0$) and panel (b) the ratios of the total norms (including all wavenumbers).

degree of approximation the evolution of the eddy part of the perturbation for about two days, from day 6 to day 8. This numerical result explains why the baroclinic instability theory, which is linear in essence, has been successful in explaining the behaviour of baroclinic waves. It should be noted that Lacarra and Talagrand (1988) also found a period of validity of 48 hours for the tangent linear model, when they investigated the short-range evolution of small perturbations in a barotropic model. Our results are also consistent with those obtained in a primitive equation model by Vukicevic (1991). At longer range, the ratio $\frac{\|\mathcal{D}\|}{\|\mathcal{L}\|}$ (full curve) increases. This comes from the saturation of the nonlinear evolution $\mathcal{N}$ while $\mathcal{L}$ exhibits an exponential growth. Furthermore, $\mathcal{D}$ has the same asymptotic behaviour as $\mathcal{L}$ since some nonlinear terms have to compensate for the linear growth in order to get a saturation of the sum. On panel (b) the ratio of the nonlinear terms ($\mathcal{D}$) to the linear term ($\mathcal{L}$) (full curve) reaches 19.9 % at the 24 h range, 38.7 % at the 48 h range and 59.0 % at 72 h. As can be seen from this figure, the total evolution of the perturbation is less linear than the evolution of the eddy part only. As the zonal flow alone is almost stationary, it is the interaction of the eddy component of the flow with the zonal part which explains this increase in nonlinearity. This result is a direct consequence of the theoretical analysis of section 2 which showed that the eddy component of the flow had no linear interaction with its zonal part.

Other results are direct consequences of the experimental set-up chosen, namely that the linearisation is performed in the vicinity of a zonal basic flow and/or that the initial perturbation at time t_0 is concentrated in wave number 6 and to a lesser extent in its harmonics. What can be seen from Fig. 4 is that the evolution of the eddy part of the perturbation is governed by odd terms, since in panel (a) $\frac{\|\mathcal{D}\|}{\|\mathcal{L}\|}$ (full curve) and $\frac{\|\mathcal{O}\|}{\|\mathcal{L}\|}$ (dotted curve) are almost identical. It means that the evolution of the eddy part of the flow is nearly the opposite when starting from $x_0(t_0) - \delta x(t_0)$ rather than $x_0(t_0) + \delta x(t_0)$. The explanation lies in the fact that almost all the energy of the non zonal components of the flow is concentrated in one single wavenumber: zonal wavenumber six (more than 99% of the total energy). Taking plus or minus the perturbation then simply consist in rotating the whole structure by half a wavelength i.e. $\frac{\pi}{6}$ in longitude. However, this is not strictly true since in the initial conditions (day 6 of the life cycle), and during the nonlinear integration, the harmonics 12 and 18 are also excited although their amount of energy is negligible (respectively 3 and 8 orders of magnitude smaller than in zonal wavenumber 6). This explains the presence of non-zero even terms in the difference $\mathcal{D}$ of panel (a) between the nonlinear evolution of the perturbation and its linear evolution (dashed curve).

The same argument can explain why the retroaction of the wave on the zonal part of the flow is almost of even nature. Due to the symmetry of the problem, a simple rotation in longitude of the eddy pattern does not alter its contribution to the zonal changes. Curve $\frac{\|\mathcal{E}\|}{\|\mathcal{L}\|}$ of panel (b) confirms the result and reveals the importance of these even contributions. Accordingly, $\frac{\|\mathcal{O}\|}{\|\mathcal{L}\|}$ is unchanged with respect to panel (a).

It should be stressed that these results, namely the fact that the evolution of the amplitude of the wave is governed by odd terms and that the feedback of the wave on the zonal flow is even with respect to the eddy part of the flow is perfectly consistent with simple nonlinear models representing baroclinic instability (see for example

Pedlosky (1970) for the finite-amplitude behaviour of unstable baroclinic waves in a quasi-geostrophic two-layer model). However, the curves of Fig. 4 can be reproduced from this theoretical model only with an e-folding time of the linear amplification of the baroclinic wave half of what observed in the multilevel primitive-equation model. This shows that the dynamics involved in our experiments are far more complicated and cannot be reduced to simple theoretical models. In particular, barotropic effects cannot be neglected.

4 Assimilation experiments.

4.a The experiments.

The assimilation problem is to find the initial conditions for a numerical forecast, taking into account all the prior information on the atmospheric state. 4D-VAR approach consists in using the dynamical information through the model equations by finding the model trajectory which is closest to the available data over a certain time period (t_0, t_n) before the beginning of the forecast.

In the following, the assimilation period generally spans 24 hours from day 6 to day 7, during which the cyclogenesis is the most intense. The observations are extracted from model states in spectral space, obtained from the reference trajectory given by the fifteen-day run. In this adiabatic problem, they simply consist of the spectral components of vorticity, divergence, temperature and of the logarithm of the surface pressure. We assume that observations are available at every time step, i.e. at a frequency of forty minutes in truncation T21.

The cost function to be minimized is

$$J(x(t_0)) = \frac{1}{2}\sum_{i=0}^{n} < x(t_i) - x_{ref}(t_i), x(t_i) - x_{ref}(t_i) > \qquad (11)$$

where $x(t_i)$ stands for the model state at time t_i and $x_{ref}(t_i)$ for the reference state at the same time. The inner product is the one associated with the norm energy given by Eq. 10. In the experiments, in which only part of the flow is supposed to be observed, only certain spectral components will be taken into account in this cost function. The inner product energy is also used for defining the metric in the minimization space. The minimization algorithm is of a mixed quasi-Newton / conjugate gradient type (Buckley and Lenir, 1983).

4.b Observation of the evolution of the eddy part of the flow.

The purpose of this first series of experiments is to test the assimilation method in a "theoretical" situation where the eddy part of the flow is assumed to be observed whereas the zonal part of the flow is not. Artificial as such a choice may appear, it has a meteorological significance. Ground-based observing networks depict reasonably well the eddies over the continents but lack of observations over the oceans often fails to give a satisfactory description of large-scale structures such as the midlatitudes upper jets.

For the different variables, the observations consist of all the zonal wavenumbers m except $m = 0$: all but the zonal components of the flow. Is it then possible to retrieve the zonal part of the flow from the observation of the temporal evolution of the eddy part of the flow?

In a first experiment the initial point of the minimization is the atmospheric state at day 4 (Fig. 6), whose zonal part is significantly different from the desired result (Fig. 5) although its structure is comparable. The main differences between the two fields are located at the lowest levels. At day 6, winds have become stronger below the jet and easterlies have spread on both sides of it. Between day 4 and day 6 the maximum

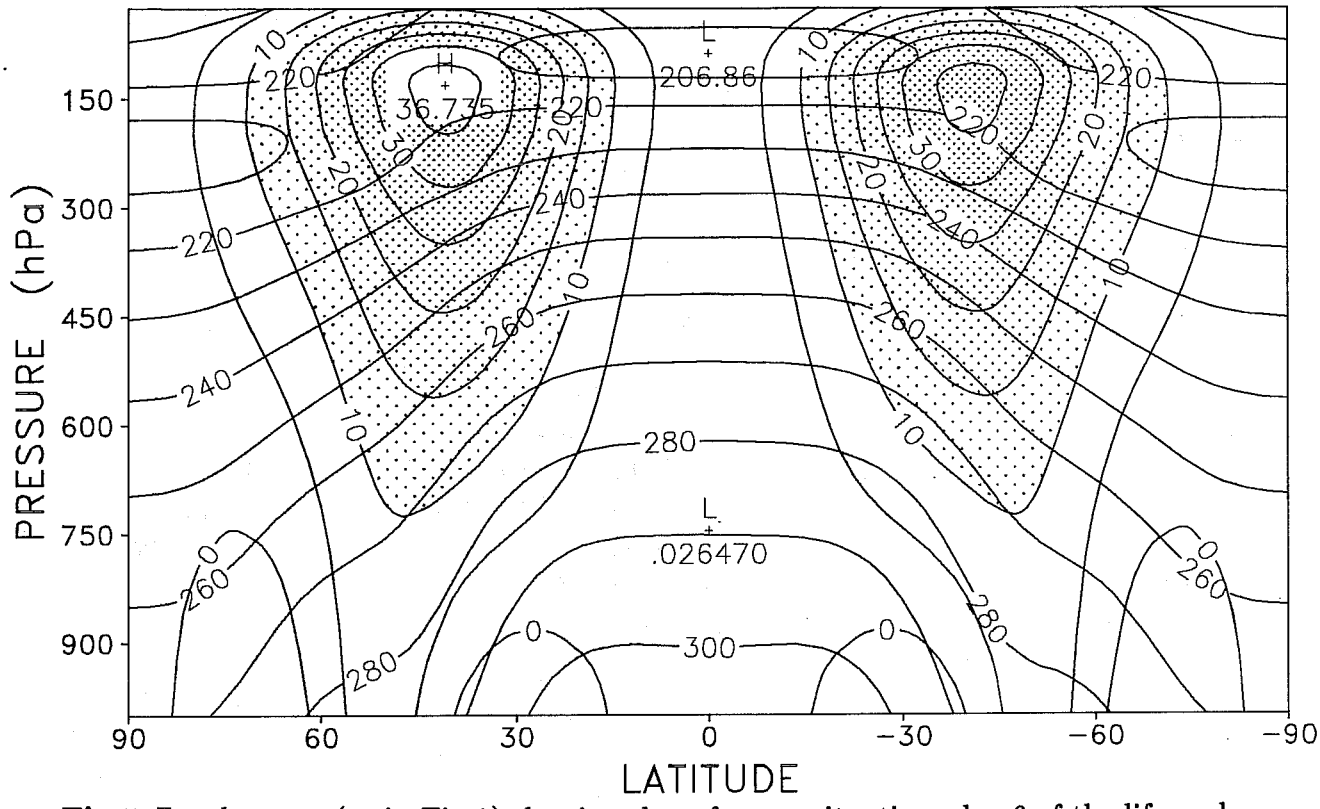

Fig.5 Zonal means (as in Fig.1) showing the reference situation: day 6 of the life cycle.

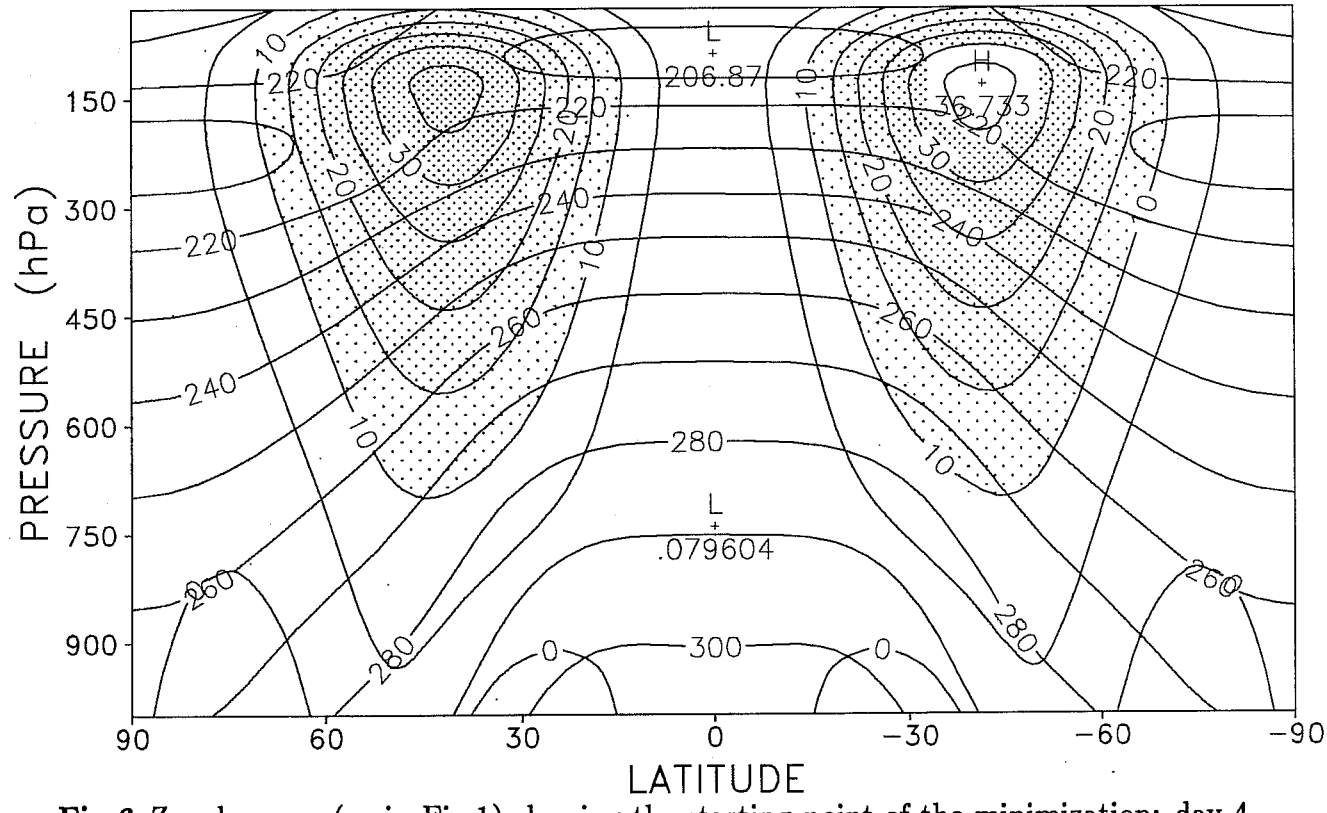

Fig.6 Zonal means (as in Fig.1) showing the starting point of the minimization: day 4 of the life cycle.

difference in zonal winds is $2.90ms^{-1}$, and in temperature $2.37K$. The algorithm performs well; the cost function is reduced by 5 orders of magnitude after 30 iterations and the global distance between the zonal part of the result and the truth is reduced by a factor of 2.4. Fig. 7 compares well with reality (Fig. 5). Winds exceeding $5ms^{-1}$ now reach the ground at midlatitudes.

The next step is to start the minimization from an atmospheric state much different from the reference one, taking a state of rest with the standard atmospheric structure of temperature and a uniform standard pressure. The maximum difference now reaches $36ms^{-1}$ in zonal winds, and $18K$ in temperature. When performing the assimilation, the convergence is very slow. No less than 150 simulations are necessary to reach a relative saturation of the minimization. The problem beneath this slowness is the fact that two distinct parts of the control variable are treated jointly: the eddy part of the flow, which is fully observed, and the zonal part of the flow for which the information is indirect through dynamical links. Treating two components of the control variable that have such different impacts on the cost function leads to a classical narrow-valley conditioning problem. To speed up convergence we chose to perform the minimization only with respect to the zonal part of the flow, the eddy part being set equal to truth at the beginning of the minimization. From Fig. 8 (to be compared to Fig. 5) one sees that the result of the minimization after 90 simulations is quite encouraging. The important features of the flow at mid-latitudes, i.e. the tropospheric jet in conjunction with the thermal meridional gradient are reproduced. However, differences can be seen in the tropics at low levels and at high latitudes. An important issue is whether this poor reconstruction of the flow at the poles and the tropics is inherent to the information contained both in the observations and in the dynamics or whether it is an artefact of this particular simulation. In order to have a clear idea of what we can expect from the algorithms independently from the starting point of the minimization we evaluate the Hessian matrix of the cost function which represents the inverse of the analysis error covariance matrix at the minimum (see Thépaut and Moll, 1990) as being the empirical covariance matrix of a set of 50 gradients obtained for different sets of observations (see appendix 2). In Fig. 9 the diagonal elements of the Hessian matrix corresponding to the zonal part of the wind (panel(a)) and the temperature (panel(b)) are shown. They represent the confidence that we can have in the corresponding analysis. This confidence is considerably higher at midlatitudes than anywhere else. There are at least 3 orders of magnitude between the midlatitude values and the ones at the equator or at the poles for both fields. This can be explained by the fact that the information on the zonal part of the flow is contained in the evolution (and in particular the advection) of the perturbation. As this perturbation is mainly confined to the latitudes ranging from 20° to 70°, the zonal fields are less easily reconstructed elsewhere.

Does the assimilation period length affect the results? This is investigated varying it from 12 to 72 hours. Plotting the values of the cost functions according to the number of simulations gives an idea of the rate of decrease (Fig. 10). For ranges up to 48 hours, the figure shows that the longer the assimilation period is, the better the result. This is because more information is present. For longer periods than 72 hours, section 3 has shown that nonlinearities become a dominant part of the dynamics. These nonlinearities generally induce a non-quadraticity of the cost function and thus a much more difficult

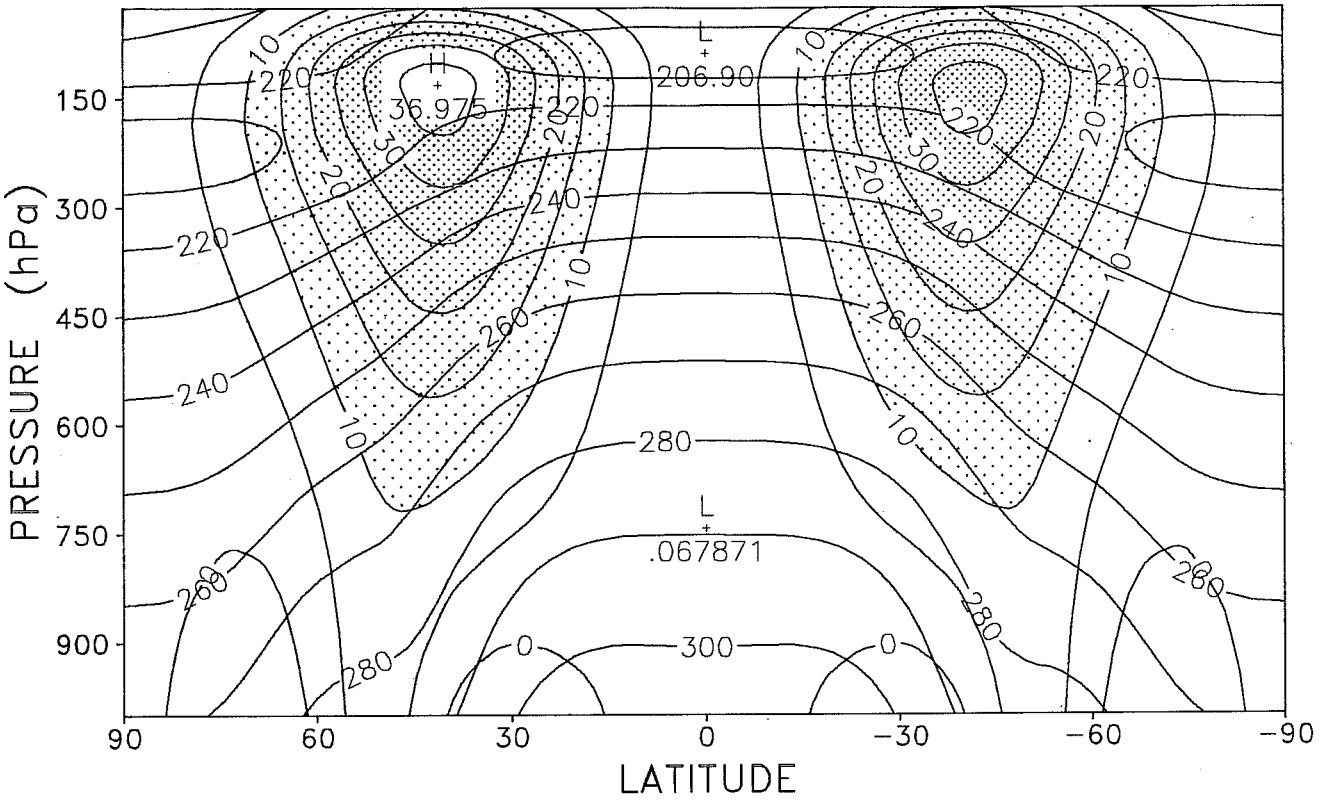

Fig.7 Zonal means (as in Fig.1) showing the result of the assimilation after 30 simulations. The starting point of the minimization is day 4. Observations consist of all zonal wavenumbers except $m = 0$ for all the model variables, at each time step for an assimilation period of 24 hours (day6 to day7).

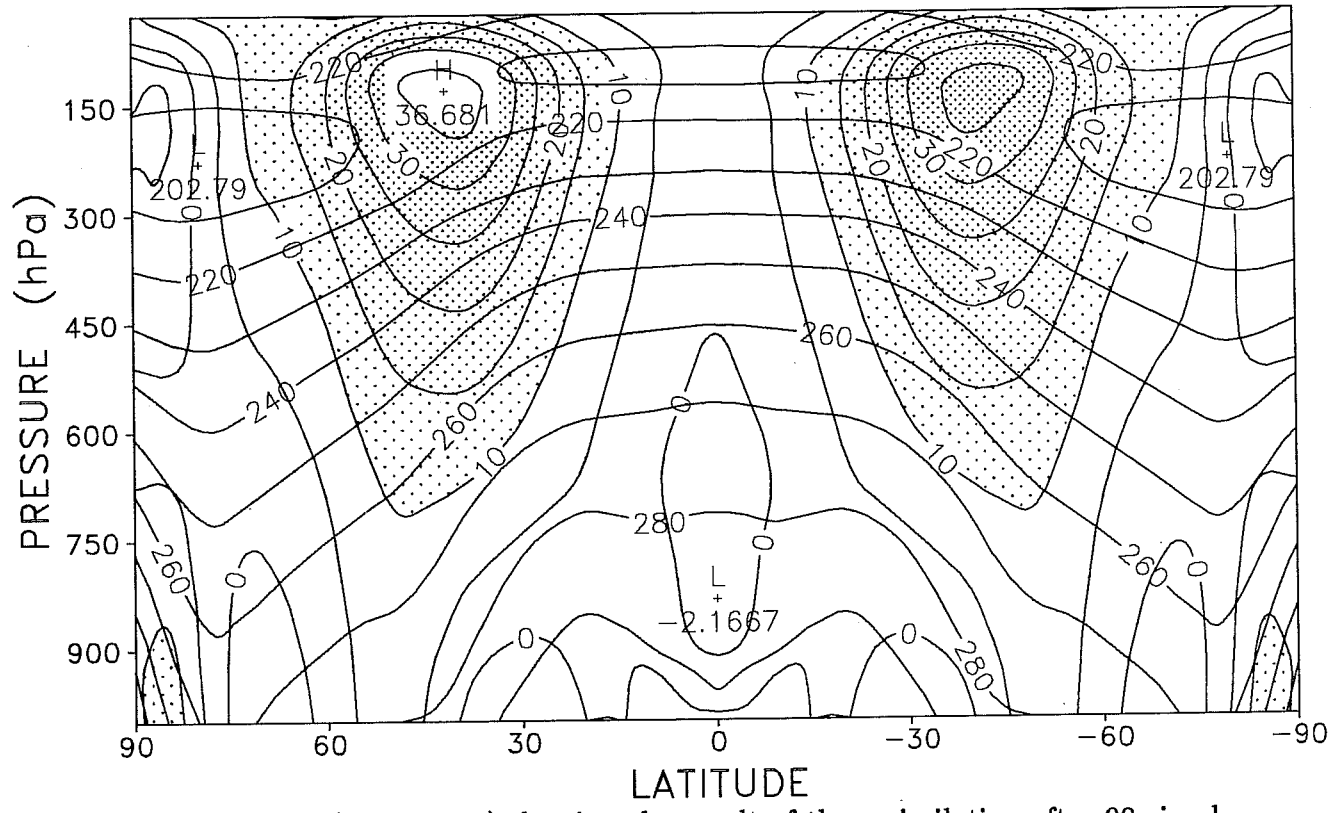

Fig.8 Zonal means (as in Fig.1) showing the result of the assimilation after 90 simulations. Starting point of the minimization: state of rest, standard temperature and standard pressure for the zonal part of the flow; the same as the reference situation for the eddy part of the flow. Observations: all zonal wavenumbers except $m = 0$ for all the model variables, at each time step for an assimilation period of 24 hours (day6 to day7). The minimization is performed only with respect to the zonal part of the flow.

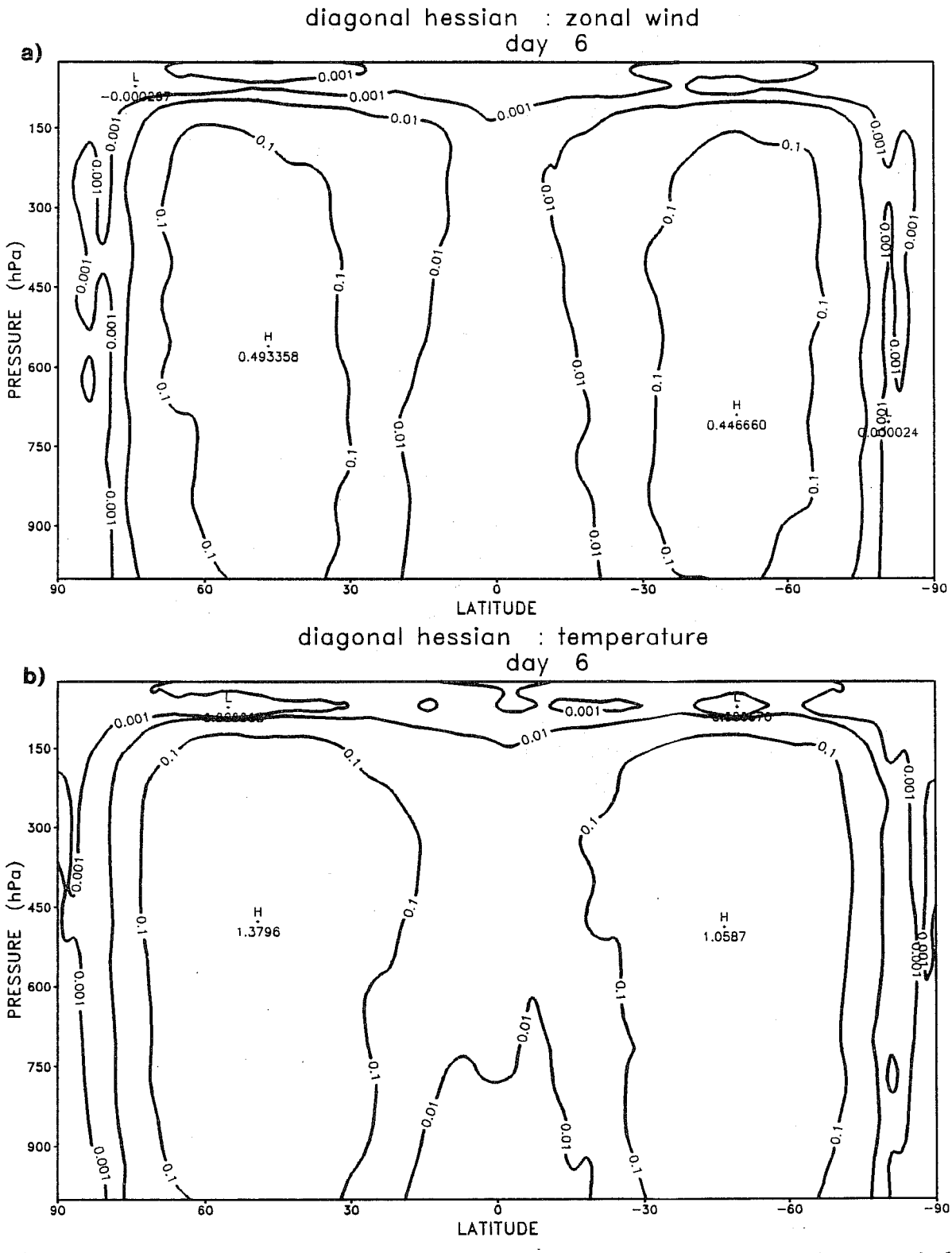

Fig.9 Diagonal elements of the Hessian matrix corresponding to the zonal mean wind (panel (a)) and zonal mean temperature (panel (b)).

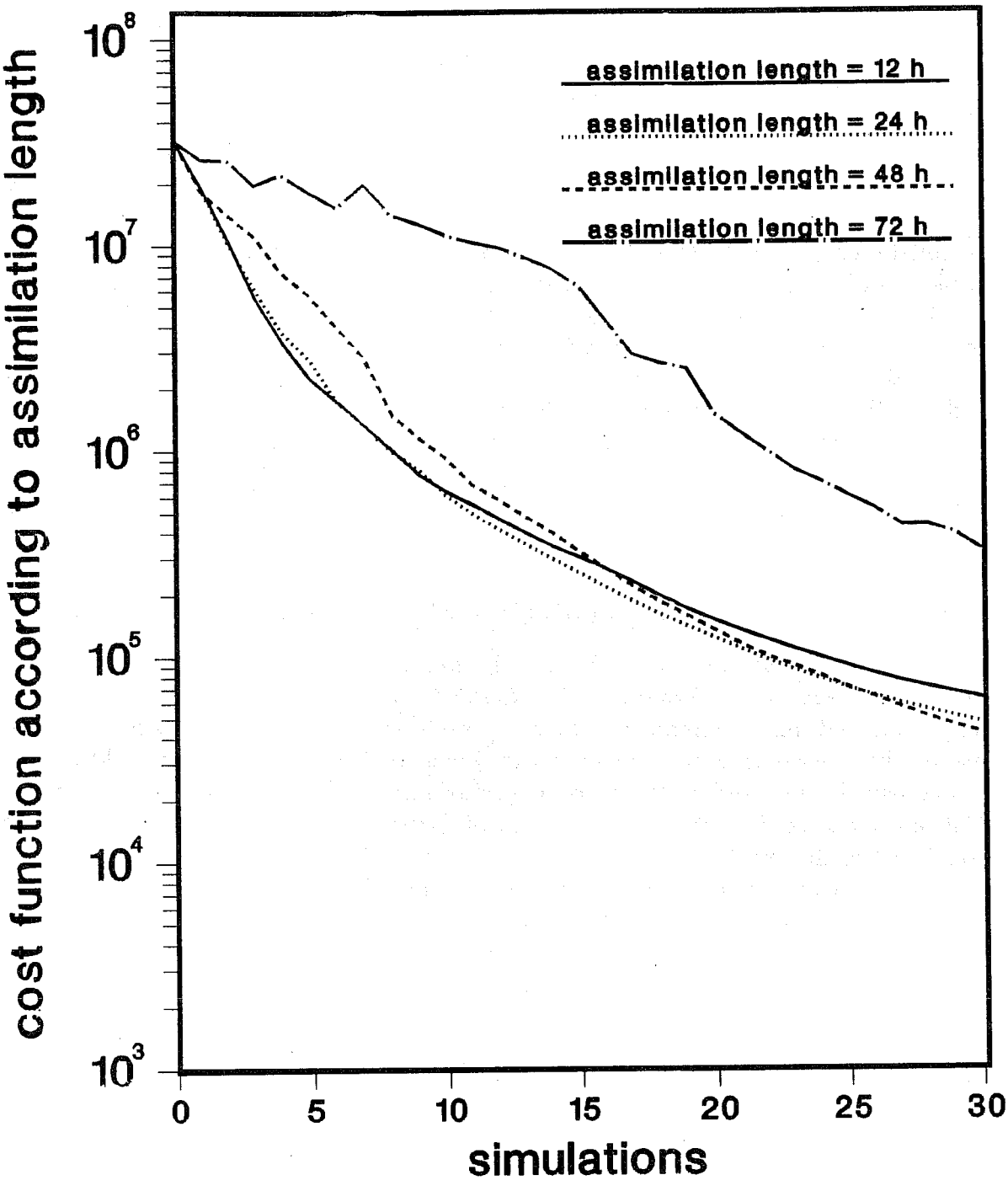

Fig.10 Values of the cost function for different assimilation period according to the number of simulations. Starting point of the minimization: state of rest, standard temperature and standard pressure for the zonal part of the flow; the same as the reference situation for the eddy part of the flow. Observations: all zonal wavenumbers except $m = 0$ for all the model variables, at each time step for an assimilation period of 24 hours (day6 to day7). The minimization is performed only with respect to the zonal part of the flow.

Full curve: assimilation period length = 12 hours

Dashed curve: assimilation period length = 24 hours

Dotted curve: assimilation period length = 48 hours

Dash-dotted curve: assimilation period length = 72 hours

The curves are scaled so as to start from the same value at the initial time of the assimilation.

minimization. This can be seen here on the behaviour of the descent algorithm which is rather erratic. Two trials are sometimes necessary for a line search along the descent direction. However, after 20 to 30 simulations, the rate of decrease is considerably higher for the 72 hour assimilation period than for the others. In contrast with what happens for the 12 hour period, minimization is far from being saturated after 30 simulations. In order to perform the experiments at a reasonable cost (around 30 to 60 simulations) assimilation periods of 24 to 48 hours seem to be a good compromise between the number of pieces of information available and the efficiency of the descent algorithm.

To summarize, the important result is that the assimilation method succeeds in reconstructing the zonal part of the fields at midlatitudes from the observation of the temporal evolution of the eddy part of the flow. However, the quality of the analysis is highly satisfactory elsewhere only if the starting point of the minimization lies within a meteorologically realistic distance from the desired minimum i.e. a few metres per second and a few Kelvin maximum differences between the fields, because of the weak dependence of the eddies upon the large-scale flow at latitudes higher the 70° or lower than 20°.

4.c Observation of the evolution of the zonal part of the flow.

Another question of interest in the assimilation of meteorological observations is addressed: can eddies be inferred from the knowledge of the time evolution of atmospheric large-scale features? Symmetrical to what was done in the previous series of experiments, the observations now include all the zonal wavenumbers of the variables except $m = 6$, which characterizes the synoptic perturbations present in the atmospheric flow. Is it possible to retrieve the eddies from the observation of the temporal evolution of the zonal part of the flow?

The first experiment, started from the atmospheric state at day 4, exhibits results which may look surprising. In Fig. 11 one clearly sees the decrease in the cost function and the paradoxical increase in the distance between the result of the minimization and reality. The interpretation can be found in Fig. 12. The eddy intensity of the result of the assimilation process is approximately correct, but the pattern is out of phase. The dynamics included in the assimilation method are able to infer the development of the perturbation from the temporal evolution of the zonal part of the flow. The minimum of surface pressure has dropped by $7hPa$ from $1003.6hPa$ in the starting point of the analysis to $996.4hPa$. However, due to the symmetry of the problem it is clear that the feedback of the perturbation on the zonal part of the flow is independent of its location in longitude. The location of the perturbation as given by the initial point of the minimization (day 4) is kept unchanged.

Now, if no information at all is given on the longitudinal location of the perturbation, either in the assimilation process or in the initial point of the minimization (the zonal part of the flow at day 6), the algorithm fails to find a minimum. This is typically a case where the cost function possesses multiple minima, as can be seen in Fig. 13 which shows a cross-section of the cost function along the direction of the perturbation. For the perturbation itself, the value is stricly zero, but for minus the perturbation (which roughly corresponds to a $\frac{\pi}{6}$ shift in longitude) the cost function is also very close to zero.

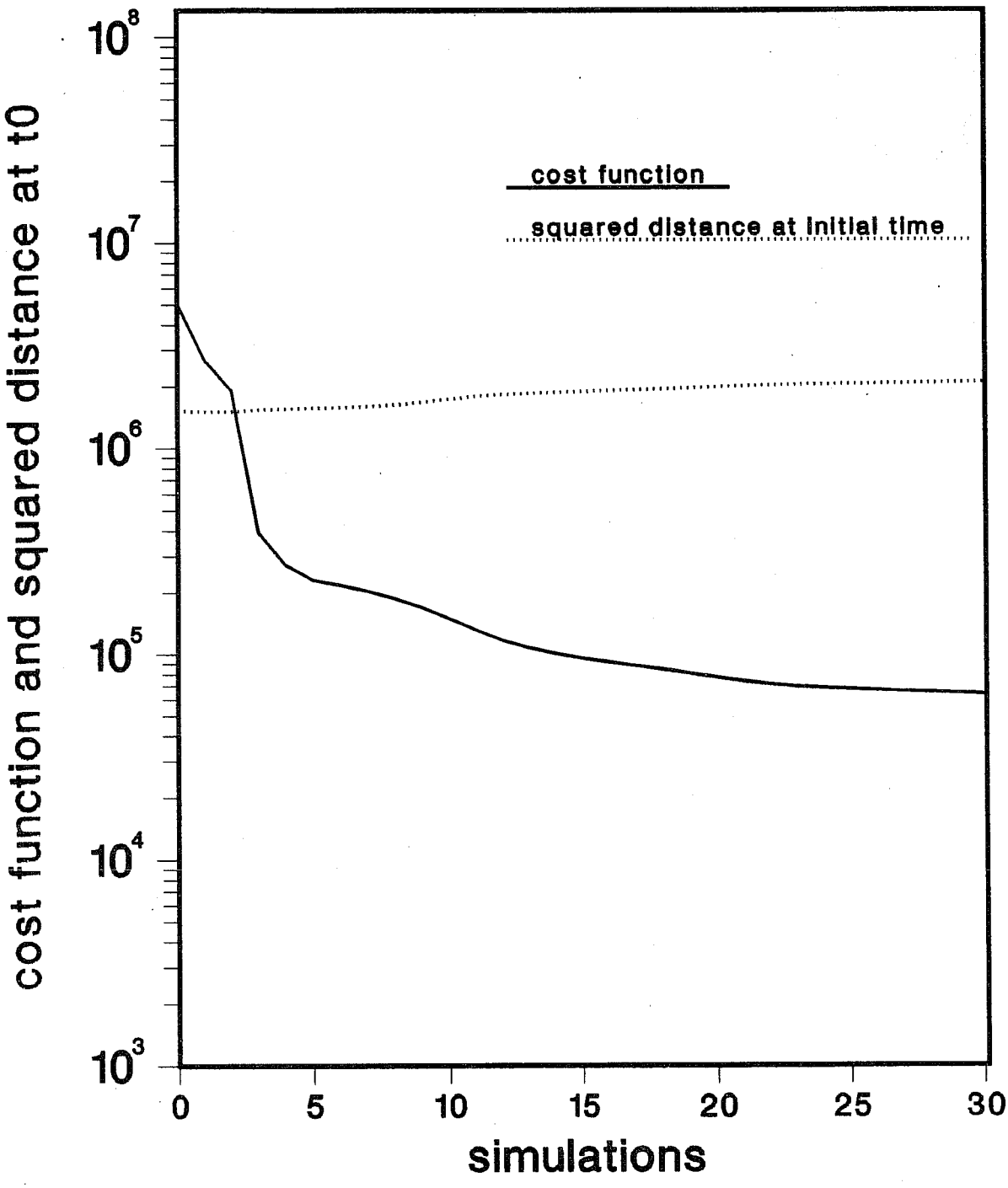

Fig.11 Values of the cost function (full curve) and of the squared distance between the result of the minimization and the reference situation (dotted curve) according to the number of simulations. Starting point of the minimization: day 4 of life cycle. Observations: all zonal wavenumbers except $m = 6$ for all the model variables, at each time step for an assimilation period of 24 hours (day6 to day7).

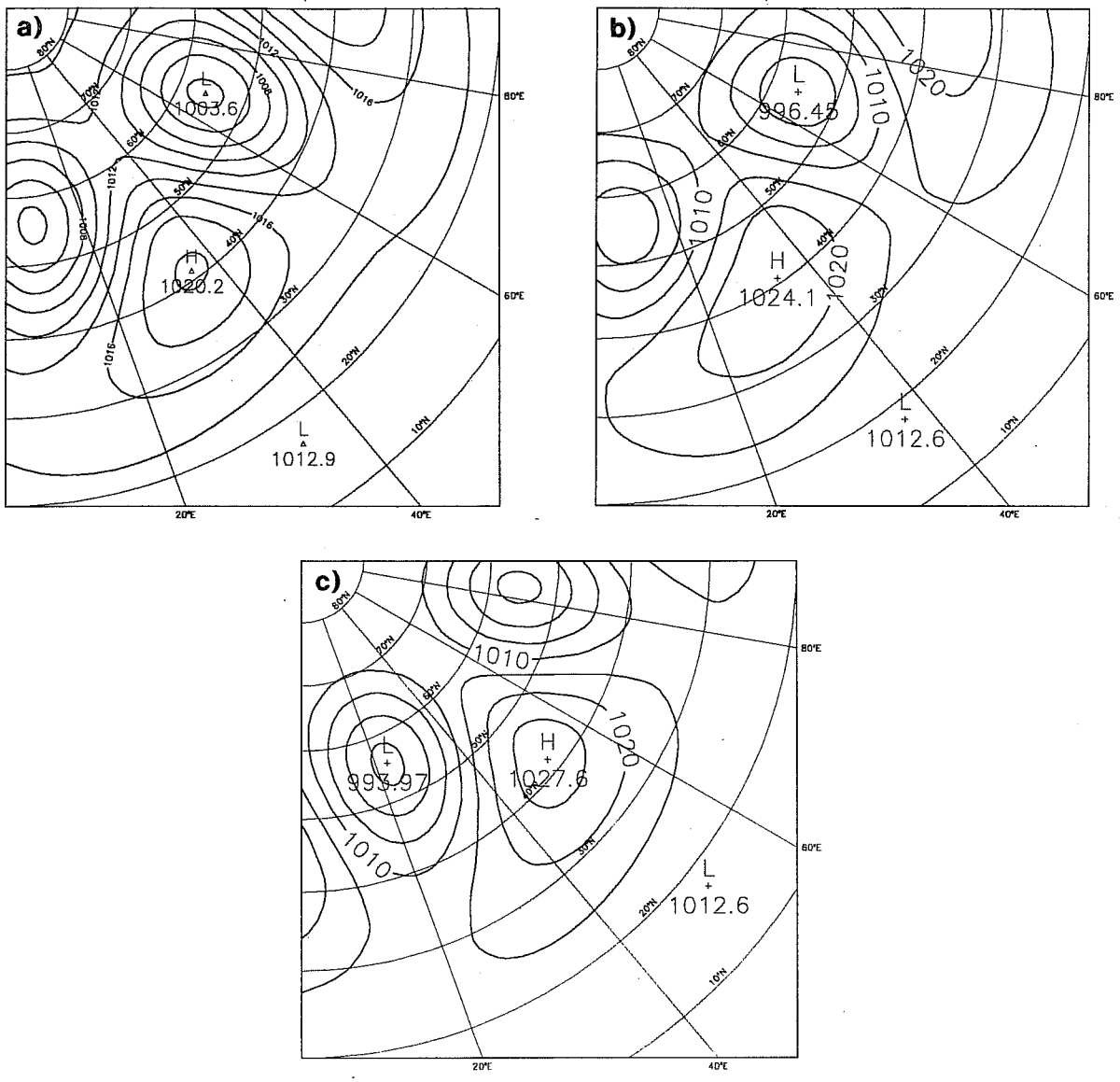

Fig.12 Results of the assimilation for the surface pressure after 30 simulations when observations consist of all zonal wavenumbers except $m = 6$ for all the model variables, at each time step for an assimilation period of 24 hours (day6 to day7).

Panel (a) shows the starting point of the minimization: day 4 of the life cycle.

Panel (b) shows the result of the minimization.

Panel (c) shows the reference field.

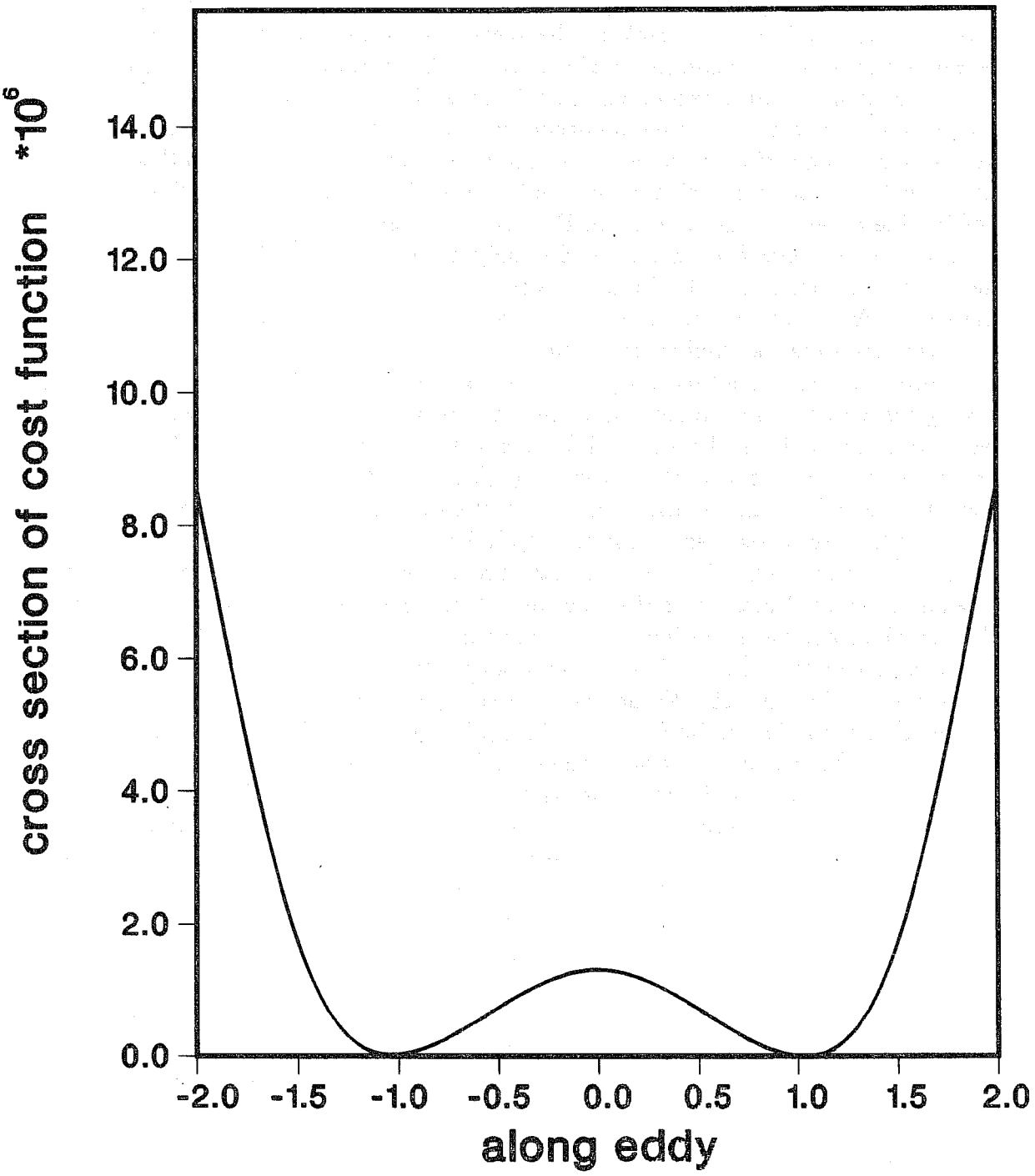

Fig.13 Cross section of the cost function along the direction of the perturbation: values of the cost function measuring the discrepancy between the reference run and the model run taking into account all components of the flow except $m = 6$, when the model is started from the zonal part of the flow at day 6 to which α times the eddy part of the flow at day 6 is added (α is shown in the abscissa).

The next experiment is designed to solve this problem of undetermined location of the perturbation with as little additional information as possible. For the three dimensional fields (vorticity, divergence and temperature) the observations are, as before, all the zonal wavenumbers except $m = 6$. But for the surface pressure, which can be considered to be well observed in the meteorological reality, the first total wavenumbers from $n = 0$ to $n = 8$ and all the zonal wavenumbers associated with them are considered to be known. It is of importance to note that observing up to $n = 8$ for the surface pressure gives information on only 36% of the energy of the perturbation of this field in this particular experiment. The starting point of the minimization is the zonal part of the flow at day 4 of the life cycle. As can be seen in Fig. 14 the results are very good. Starting from an unperturbed zonal field and observing only a part of the perturbation (panel (a)), the pattern obtained after 60 simulations (panel (b)) is in good agreement with reality (panel(c)). For the other meteorological fields, for which no eddy component is observed, the wave pattern is also well represented.

In order to generalize this study, a similar experiment is performed where, while observing basically the same quantities as in the previous experiment (i.e. zonal wavenumber $m = 0$ for the three-dimensional fields and total wavenumbers $n = 0$ to $n = 8$ for the surface pressure), the starting point of the minimization now contains some random noise in all zonal wavenumbers. This introduction of noise allows for more components of the gradient to be excited during the minimization process. It is found that after 60 simulations, the amount of energy in zonal wavenumbers 6 and its harmonics is increased to realistic values. However, as the noise introduced in other zonal wavenumbers did not affect significantly the evolution of the zonal part of the flow, it was not removed. This superposition of the wave and of the random noise clearly shows on the temperature field presented in Fig. 15. What can be concluded from this experiment is that the introduction of random noise in the starting point of the minimization does not have a detrimental effect on the retrieval of the baroclinic wave.

This series of results clearly shows the potential of 4D-VAR. The purely nonlinear feedback that exists between the perturbation and the zonal part of the flow is correctly treated. Once a piece of information on the location of the perturbation is present in the observations or in the starting point of the minimization, the full baroclinic wave is correctly derived from the temporal evolution of the zonal part of the flow.

4.d Observation of the T21 part of the flow.

What meteorologists would really appreciate from an elaborate assimilation method is to retrieve the fine-scale structure of a weather system from the observation of the large-scale pattern. This question is addressed in an experiment at truncation T42 where the starting point of the minimization is day 6 of the life cycle (at T42) truncated at T21 and the observations are the total wavenumbers $n = 0$ to $n = 21$ of the evolution of the T42 fields over a 24-hour period. Hence, the only fine-scale information introduced in the minimization is purely indirect. It is contained in the observation of the large-scale pattern which is modified through its interaction with small scales. In order to improve the conditioning, the minimization is performed with respect to the total wavenumbers $n = 22$ to $n = 42$ only.

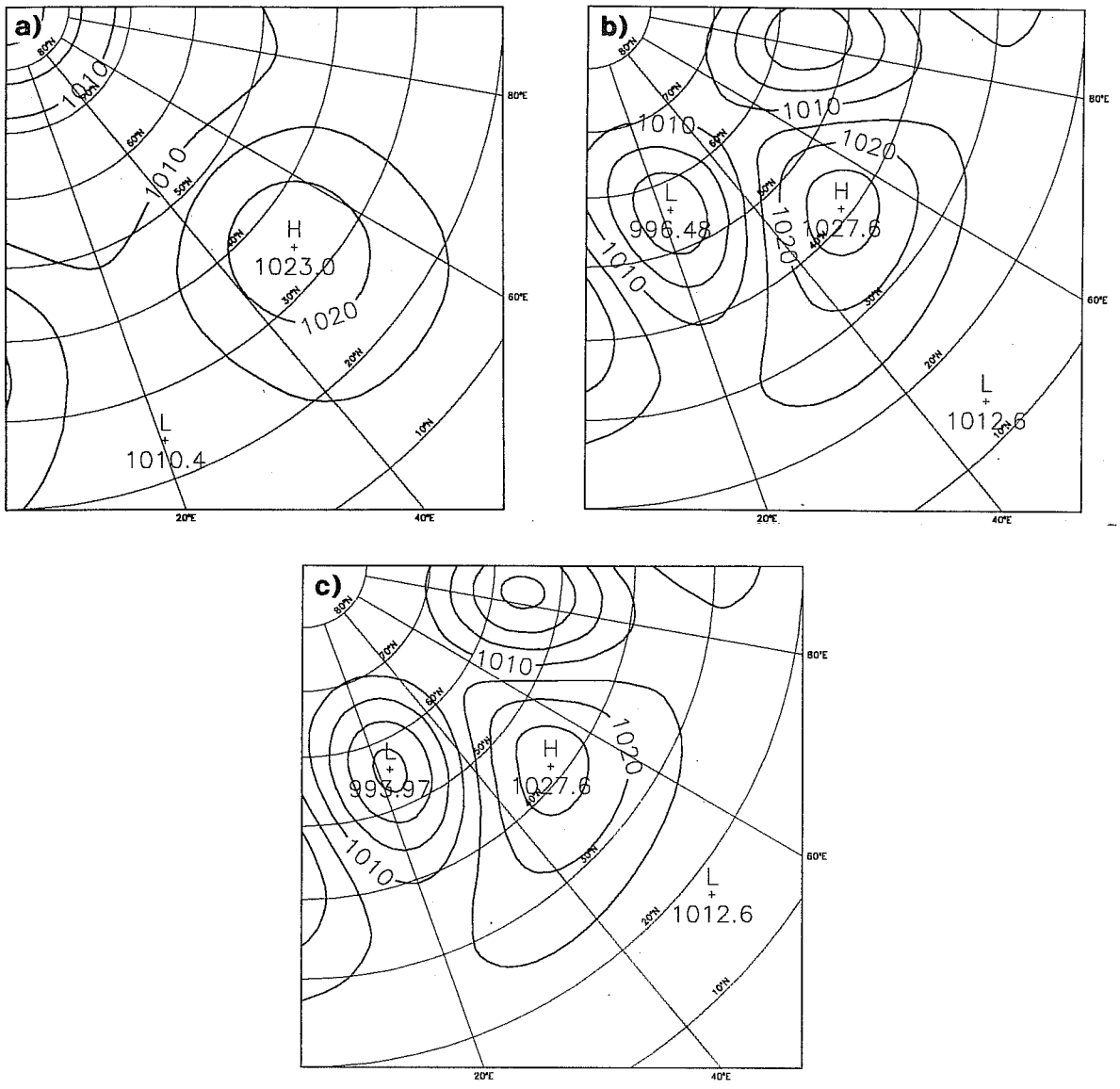

Fig.14 Results of the assimilation for the surface pressure after 60 simulations, starting from the zonal part of the flow at day 4. Observations consist of all zonal wavenumbers except $m = 6$ for all the model variables, except for the surface pressure for which all total wavenumbers from $n = 0$ to $n = 8$ (with the corresponding zonal wavenumbers) are observed. The frequency and period of observation is the same as before.

Panel (a) shows the observations for the surface pressure at the first time step.

Panel (b) shows the result of the minimization.

Panel (c) shows the reference field.

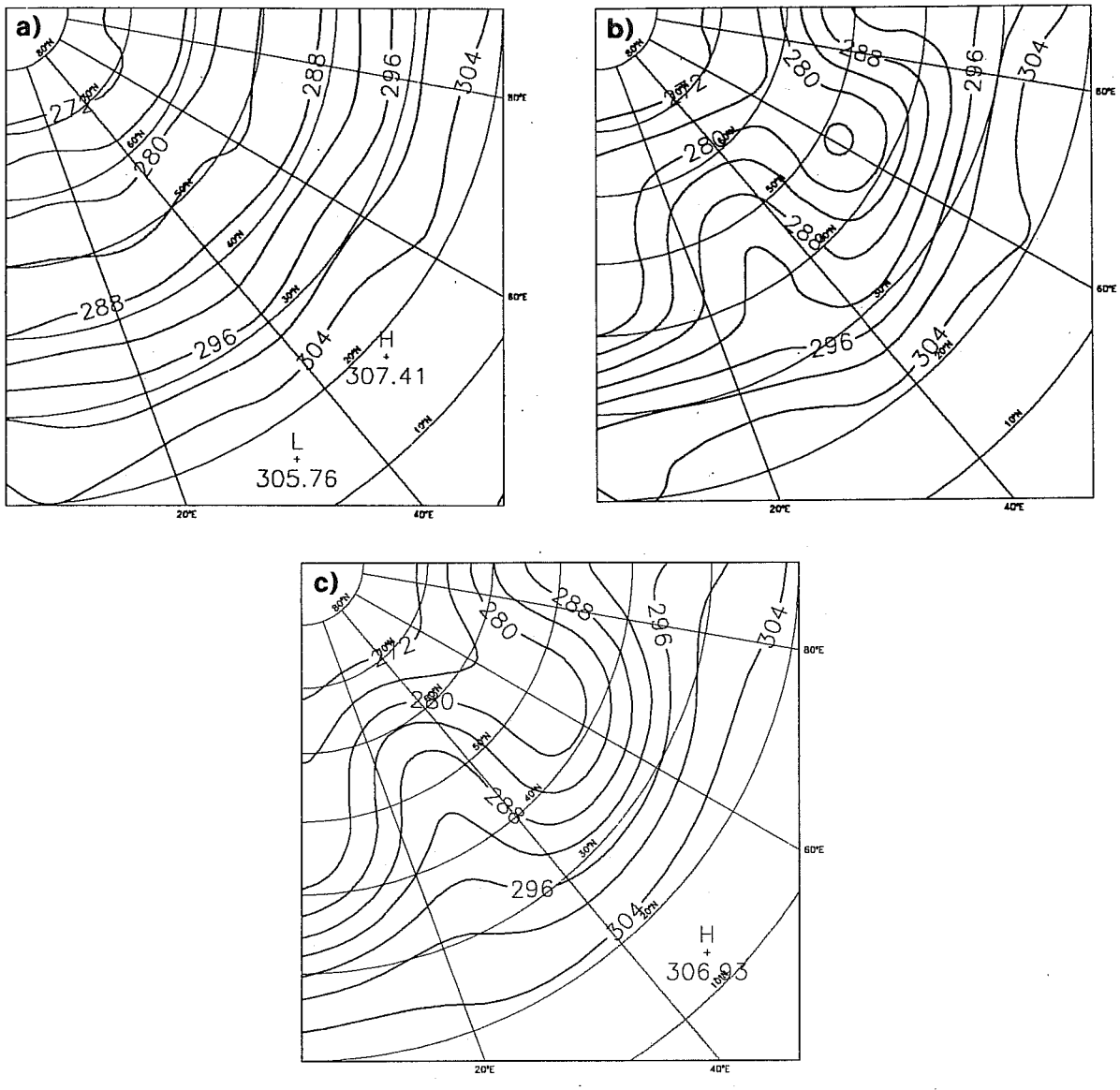

Fig.15 Results of the assimilation for the temperature at the lowest level after 60 simulations when observations consist of all zonal wavenumbers except $m = 6$ for all the model variables, except for the surface pressure for which all total wavenumbers from $n = 0$ to $n = 8$ (with the corresponding zonal wavenumbers) are observed. The frequency and period of observation is the same as before.

Panel (a) shows the starting point of the minimization: day 4 of the life cycle to which a random noise is added.

Panel (b) shows the result of the minimization.

Panel (c) shows the reference field.

Fig. 16 shows which portion of the total energy can be retrieved after 30 descent steps. As already found in TC91 it is more difficult to retrieve the small scales from the observation of the large scales than the opposite; the agreement between the two spectra is far from being perfect. However, it is clear that some information has been recovered. This could also be seen in the regular decrease of the distance to the truth which had been divided by a factor of 2.2 (not shown). It should be noted that the fact that the length of the assimilation period is 24 hours in this experiment helps to have a stronger dependence between the large and the fine scales than in TC91. When the same experiment is run with an assimilation period length of 6 hours only, the results are slightly worse (the decrease does not exceed 2.0).

Looking at the surface pressure charts in Fig. 17, one can see that in both experiments the pronounced gradients in the vicinity of the low and the trough at 20° E (panels (b) and (c)), which were not present in the starting point of the minimization (panel (a)), are now in good agreement with the T42 reference field (panel (d)). The main noticeable difference between the two experiments is that, for the 24-hour assimilation period, the extreme values of the low and of the high are closer to reality than for the 6-hour assimilation period length.

Of course, the particular framework chosen in this study contains only one weather system and may have simpler dynamics than a full meteorological situation. This prevents us from hastily concluding that small scales can be retrieved from the observation of the large scales. Still, these results are a strong indication that, for a realistical assimilation period and in so far as the conditioning of the problem is correct, valuable information can be retrieved on the small scales through the dynamical information.

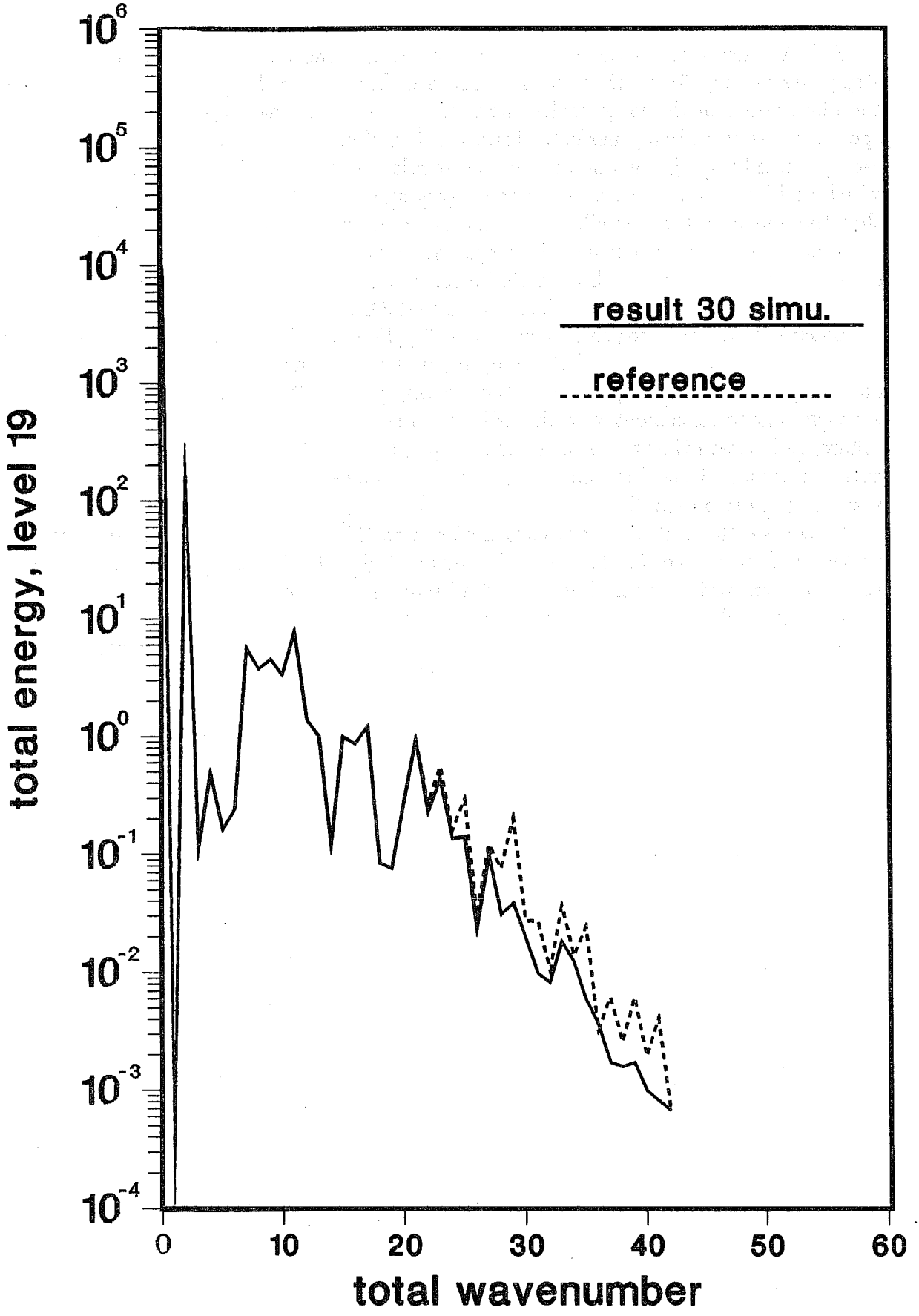

Fig.16 Spectra of energy at the lowest level of the model for the starting point of the minimization (dotted curve) and for the result of the minimization after 30 simulations (full curve). The starting point of the minimization is the zonal part of the flow at day 4 of the life cycle to which a random noise has been added. The observations are the same as in the previous experiment.

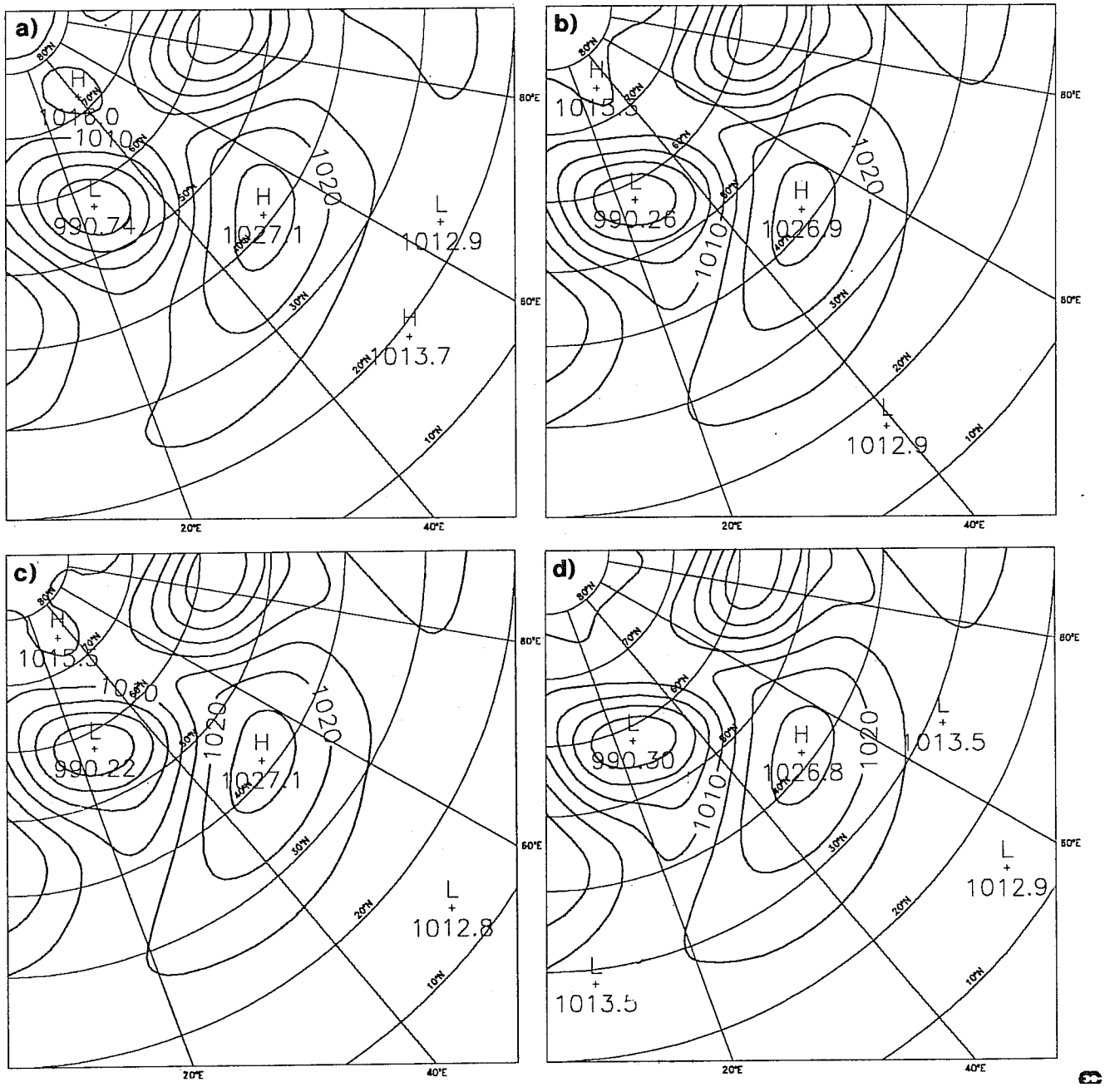

Fig.17 Results of the assimilation for the surface pressure after 30 simulations when observations consist of all total wavenumbers from $n = 0$ to $n = 21$.

Panel (a) shows the starting point of the minimization: day 6 of the life cycle at T42 truncated at T21.

Panel (b) shows the result of the minimization for a 24-hour assimilation period length.

Panel (c) shows the result of the minimization for a 6-hour assimilation period length.

Panel (d) shows the reference field.

5 Discussion.

Four results have been presented in this paper addressing the problem of understanding the behaviour of four-dimensional variational assimilation in a simplified baroclinic instability context.

Firstly, the evolution of a large scale baroclinic perturbation is essentially linear within a 1-2 day range for its eddy part, whereas the modifications of the zonal part of the flow due to the wave are representative of a purely nonlinear zonal-eddy coupling. The linearity of the eddy evolution should be investigated at higher resolution and in particular in secondary cyclogenesis as in Thorncroft and Hoskins (1990) where breaking phenomena occur.

Secondly, the observation of the evolution of the eddy component of the flow is enough to infer the zonal part of the flow at midlatitudes, if the starting point of the minimization is close to the minimum. However, convergence can be considerably slower if one starts the minimization very far away from the desired result or when the problem is dominantly nonlinear i.e. if the assimilation period length exceeds the range of validity of the tangent linear approximation.

Thirdly, the observation of the evolution of the zonal part of the flow is enough to infer the eddy component in two cases: (i) if the starting point of the minimization is at a meteorologically reasonable distance from the truth (two days apart) or (ii) if one also observes the very large scale pattern of the surface pressure. On the other hand, if the starting point is too far away and in this particular case far outside the range of validity of the tangent linear approximation, there may be no convergence at all.

Last, but not least, in a T42 experiment the observation of the T21 evolution of the flow allows us to infer most of the higher resolution T21-T42 component of the flow.

These results illustrate the importance of the tangent linear approximation for a successful implementation of a 4-D VAR approach but also demonstrate the power of the method. The natural continuation of this work is the specification of observations in gridpoint space in order to understand which information is the most valuable in order to reconstruct a baroclinic wave using a meteorological (e.g. radiosonde) network. Once this further stage has been achieved in the understanding of the behaviour of 4-D VAR, we shall eventually proceed to the analysis of a real case like the storm of 15-16 October 1987.

6 Acknowledgments.

The authors would like to thank Olivier Talagrand (LMD), Jean Pailleux and Jean-Noël Thépaut for their helpful comments. It is also a pleasure to thank the ARPEGE/IFS team and in particular Mats Hamrud.

7 Appendix 1: theoretical results on the tangent linear model.

Let us consider the tangent-linear model obtained by linearization in the vicinity of a trajectory $x(t)$. Assuming that the initial conditions of the trajectory $x(t_0)$ consists of zonal fields, which properties can be derived for the tangent linear model ?

A first remark is that as the nonlinear equations are invariant under any zonal rotation, $x(t)$ remains zonal during the nonlinear integration. The tangent-linear equations are then invariant under any zonal rotation R_z^θ of angle θ which means that the resolvent $\mathcal{R}(t_n, t_0)$ commutes with R_z^θ : it is equivalent either to rotate the initial conditions $\delta x(t_0)$ or the result of the tangent linear equation : $\delta x(t_n) = \mathcal{R}(t_n, t_0)\delta x(t_0)$. Therefore

$$R_z^\theta \mathcal{R}(t_n, t_0) = \mathcal{R}(t_n, t_0) R_z^\theta \tag{12}$$

Second remark. A property of two linear operators $\mathcal{L}_1$ and $\mathcal{L}_2$ which commute is that any eigen-subspace E_Λ corresponding to the eigen-value Λ of $\mathcal{L}_1$ is invariant by $\mathcal{L}_2$. If y belongs to E_Λ, we have then to show that $\mathcal{L}_2 y$ also belongs to E_Λ. As y is eigen-vector for the eigen-value Λ, we have :

$$\mathcal{L}_1 y = \Lambda y \tag{13}$$

applying $\mathcal{L}_2$ on both side, we obtain :

$$\mathcal{L}_2 \mathcal{L}_1 y = \mathcal{L}_2 \Lambda y \tag{14}$$

Using the fact that $\mathcal{L}_1$ and $\mathcal{L}_2$ commute for the left hand side and the linearity of $\mathcal{L}_2$ for the right hand side, we get :

$$\mathcal{L}_1 \mathcal{L}_2 y = \Lambda \mathcal{L}_2 y \tag{15}$$

which means that $\mathcal{L}_2 y$ is eigen-vector for the eigen-value Λ and thus belongs to E_Λ.

Third remark. The rotation R_z^θ admits as eigen-vectors the spherical harmonics $Y_n^m = e^{im\lambda} P_n^m(\mu)$ with $e^{im\theta}$ as eigen value :

$$\begin{aligned} R_z^\theta Y_n^m &= e^{im(\lambda+\theta)} P_n^m(\mu) && (16) \\ &= e^{im\theta} Y_n^m && (17) \end{aligned}$$

where λ and μ are respectively the longitude and the sine of the latitude, and the P_n^m are the associated Legendre functions of second kind. This shows that when the angle θ is not in a fractional ratio with 2π, each eigen-space of the rotation R_z^θ consists of the subspace spanned by the spherical harmonics of given zonal wave number m. We shall denote in the following by E_m the subspace consisting of model state of zonal wave number m, subspace of the linear space E of all model state. When $\theta = \frac{2\pi}{n}$, the n eigen-spaces consist of $E_{m+6k}, k = 0, 1, 2, ...$ for m varying between 0 and $n-1$

Combining the three above results, it is concluded that the resolvent $\mathcal{R}(t_1, t_0)$ keeps invariant any E_m. In other words, the dynamics of the tangent linear equation obtained

by linearization in the vicinity of a zonal trajectory is independent from one m to another, and the matrix of the resolvent is block diagonal.

8 Appendix 2: relationship between analysis error covariance matrix and Hessian matrix.

Let us write the cost-function as

$$J(X_0) = \frac{1}{2}\sum_{i=0}^{n}(\mathcal{M}(t_i,t_0)X_0 - Y_i)^t Q^{-1}(\mathcal{M}(t_i,t_0)X_0 - Y_i) \tag{18}$$

where $\mathcal{M}(t_i,t_0)$ represents the integration of the model from the initial conditions X_0 at time t_0 up to time t_i, Y_i stands for the observations at the same time and Q is the matrix defining the scalar product $< .,. >$ used in 11 interpreted here as the covariance matrix of observation error:
the observations Y_i at each time step are of the form

$$Y_i = X_{it} + \epsilon_i \tag{19}$$

where the subscript t stands for true, and the observational errors (ϵ_i; i=1,n) satisfy the relations

$$\left.\begin{array}{l} E(\epsilon_i) = 0 \\ E(\epsilon_i\epsilon_i^t) = Q \\ E(\epsilon_i\epsilon_j^t) = 0 \end{array}\right\} \tag{20}$$

The gradient (first derivative of J) with respect to the Euclidean inner product can be written

$$\nabla_{X_0} J = \sum_{i=0}^{n}\mathcal{R}(t_i,t_0)^t Q^{-1}(\mathcal{M}(t_i,t_0)X_0 - Y_i) \tag{21}$$

and the Hessian matrix

$$J'' = \sum_{i=0}^{n}\mathcal{R}(t_i,t_0)^t Q^{-1}\mathcal{R}(t_i,t_0) + \sum_{i=0}^{n}\mathcal{H}(t_i,t_0)^t Q^{-1}(\mathcal{M}(t_i,t_0)X_0 - Y_i) \tag{22}$$

where $\mathcal{R}(t_i,t_0)$ represents the first derivative of $\mathcal{M}$ (tangent linear model) and $\mathcal{H}(t_i,t_0)$ the second derivative of $\mathcal{M}$.
Since the tangent linear model $\mathcal{R}$ is a good approximation to $\mathcal{M}$, the Hessian matrix reduces to

$$J'' = \sum_{i=0}^{n}\mathcal{R}(t_i,t_0)^t Q^{-1}\mathcal{R}(t_i,t_0) \tag{23}$$

and the gradient of J is zero. Using the expression of Y_i and the tangent linear approximation, one gets

$$\sum_{i=0}^{n}\mathcal{R}(t_i,t_0)^t Q^{-1}(\mathcal{R}(t_i,t_0)(X_0 - X_{0t}) - \epsilon_i) = 0 \tag{24}$$

which can be inverted in order to get the difference between the analysed state and the truth

$$X_0 - X_{0t} = (\sum_{i=0}^{n} \mathcal{R}(t_i, t_0)^t Q^{-1} \mathcal{R}(t_i, t_0))^{-1} . (\sum_{i=0}^{n} \mathcal{R}(t_i, t_0)^t Q^{-1} \epsilon_i) \tag{25}$$

Thus, the error covariance matrix at the minimum is

$$E((X_0 - X_{0t})(X_0 - X_{0t})^t) = (\sum_{i=0}^{n} \mathcal{R}(t_i, t_0)^t Q^{-1} \mathcal{R}(t_i, t_0))^{-1} \tag{26}$$

and the following relationship applies:

$$E((X_0 - X_{0t})(X_0 - X_{0t})^t) = (J'')^{-1} \tag{27}$$

In order to evaluate the Hessian matrix, we can, as in Gauthier(1990) consider the gradient as a random variable due to the observational errors. Replacing Y_i by its expression (Eq. 19) and defining the "true" gradient by

$$\nabla_{X_0} J_t = \sum_{i=0}^{n} \mathcal{R}(t_i, t_0)^t Q^{-1} (\mathcal{M}(t_i, t_0) X_0 - X_{it}) \tag{28}$$

one obtains

$$\nabla_{X_0} J = \nabla_{X_0} J_t - \sum_{i=0}^{n} \mathcal{R}(t_i, t_0)^t Q^{-1} \epsilon_i \tag{29}$$

The gradient error covariance may then be written as

$$E((\nabla_{X_0} J - \nabla_{X_0} J_t)(\nabla_{X_0} J - \nabla_{X_0} J_t)^t) = \sum_{i=0}^{n} \mathcal{R}(t_i, t_0)^t Q^{-1} \mathcal{R}(t_i, t_0) = J'' \tag{30}$$

In practice, we create 50 sets of observations with errors having the appropriate error covariance of Q, and we compute the empirical gradient error covariance to evaluate the Hessian.

9 References.

Buckley, A. and A. Lenir, 1983: QN-like Variable Storage Conjugate Gradients. *Mathematical Programming*, **27**, 155-175.

Courtier, P., C. Freydier, J-F Geleyn, F. Rabier and M. Rochas 1991: The ARPEGE Project at Meteo-France. *ECMWF Seminar proceedings, September 1991.*

Gauthier,P. 1991: Chaos and quadri-dimensional data assimilation : a study based on the Lorenz model. To appear in *Tellus.*

Gill A.E., 1982: Atmosphere-Ocean Dynamics. *Academic Press*, 662pp.

Jarraud, M., J.Goas and C.Deyts, 1989: Prediction of an exceptional storm over France and Southern England (15-16 October 1987). *Wea. For.*, **4**, 517-536.

Lacarra, J.F. and O. Talagrand, 1988: Short range evolution of small perturbations in a barotropic model. *Tellus*, **40A**, 81-95.

Lorenc, A.C., R.S.Bell, T.Davies and G.J.Shutts, 1988. Numerical forecast studies of the October 1987 storm over southern England. *Meteorol. Magazine*, **117**, 118-130.

Navon, I.M., X. Zou, K. Johnson, J. Derber and J. Sela, 1991: Variational data assimilation with an adiabatic version of the NMC spectral model. *Tech. Rep. FSU-SCRI-91-13, Tallahassee, FL 32306-4052*, 43 pp.

Pedlosky, J., 1970: Finite-Amplitude Baroclinic waves. *J.Atmos.Sci.* **27**, 15-30.

Simmons, A. and D.Burridge, 1981: An energy and angular momentum conserving vertical finite difference scheme and hybrid vertical coordinates. *Mon.Wea.Rev.*, **109**, 758-766

Simmons, A.J. and B.J.Hoskins, 1978: The Life Cycles of Some Nonlinear Baroclinic Waves. *J. Atmos. Sci.*, **35**, 414-431.

Thépaut, J.N. and P.Courtier, 1991: Four dimensional variational data assimilation using the adjoint of a multilevel primitive equation model . To appear in *Q. J. R. Meteorol. Soc.*. Also available from ECMWF as Technical Memorandum 178

Thépaut, J.N. and P.Moll, 1991: Variational inversion of simulated TOVS radiances using the adjoint technique. *Q. J. R. Meteorol. Soc.*, **116**,1425-1448.

Thorncroft, C.D. and B.J.Hoskins, 1990: Frontal Cyclogenesis. *J.Atmos.Sci.*, **47**, 2317-2336.

Vukicevic, T. 1991. Nonlinear and Linear Evolution of Initial Forecast Errors. *Mon. Wea. Rev.*, **119**, 1602-1611.